THE INTERACTION BETWEEN DEPLETION FLOCCULATION AND MOLECULAR LIQUID-LIQUID PHASE SEPARATION MECHANISMS

by

ANUPAM KUMAR

A thesis submitted in partial fulfillment of the requirements for the degree of

Master of Science

in

CHEMICAL ENGINEERING

Department of Chemical and Materials Engineering
University of Alberta

Abstract

There is growing interest in the formulation and application of nano colloids + non-adsorbing polymer in fields of nanomedicine, hydrocarbon production, and environmental science. Successful applications rely on a detailed understanding of the related fluid thermophysical and thermochemical properties. Polymer + solvent binary mixtures exhibit liquid-liquid phase behavior at low temperature. This behavior, driven by repulsive interactions between the globular conformation of the polymer, possess an UCEP temperature because the polymer undergoes a conformational change. From a Gibbs free energy perspective, at temperatures slightly above the UCEP temperature, a single-phase liquid is marginally stable. This phase behavior is driven by entropically favourable molecular interactions between polymer in the coil conformation and solvent molecules. Phase diagrams for nanoparticle + non-adsorbing polymer + solvent ternary mixtures typically exhibit colloid gas, G (a liquid comprising largely polymer and solvent), a colloid liquid, L (a liquid comprising largely solvent and colloid) and a colloid phase, C (a largely nanoparticle rich phase) phases. The phase behaviors GC, GL, LC and GLC at equilibrium are driven by depletion flocculation (a surface phenomenon). This work focuses on the interaction between these two phenomena – depletion flocculation and molecular liquid-liquid phase behavior based on the behavior of polystyrene + cyclohexane + nano silica particles. For example, above the UCEP temperature, even a trace mass fraction of silica nanoparticle (<0.005) destabilizes the marginally stable polystyrene + cyclohexane mixture.

The phase diagrams obtained in this work are discussed in relation to the UCEP temperature of the binary mixture polystyrene + cyclohexane (this work: 299 K). The interplay between molecular and colloidal effects leads to phase diagrams that were not previously

anticipated. Some of these phase diagrams were observed directly. Other phase diagrams were inferred from phase diagram theory as transitional when colloid solid (C) and colloid gas (G) + liquid (L) phase behaviors overlap. Above the UCEP temperature, one new phase diagram including two colloid G=L critical points on a closed loop colloid G+L region was observed experimentally. A second new phase diagram with a L+G+C region and two colloid G=L critical points is inferred, but not observed experimentally, based on this work and prior work of others. Below the UCEP temperature, one new phase diagram was observed experimentally and a second new phase diagram was inferred based on measurements in this work and phase diagram theory. Implications of these findings and priorities for further study are introduced.

Acknowledgements

I am thankful to my supervisor Dr. John M. Shaw. He quoted once- "No we don't always have to agree. We just have to do our best and present opportunities to one another. Something will stick". Words can't describe a journey of two years with countless support and motivations from Dr. Shaw. Thank you.

Mildred Becerra, a person who is more like a mother to me, encouraged me, trained me doing experiments in lab, supported me and made me feel like Edmonton is my second home. She is an expert lab manager and a great mentor to me.

My mom, dad and siblings always loved me and supported me. I am so fortunate to have them in my life.

Table of Contents

List of Tables

List of Figures

Chapter 1. Introduction

1.1   Formulations of Non-Adsorbing Polymer + Nano Colloid Mixtures

The physics of colloid particles + non-adsorbing polymer molecules in a good solvent is well established.[1,2] The non-adsorbing polymer molecules induce an attractive potential between colloid particles driven by an osmotic pressure difference in the solvent. The attractive potential leads to the depletion of free volume between particles and phase separation is observed. This mechanism, depletion flocculation, attracts applications and formulations in the diverge fields of hydrocarbon processing, medicine and environmental science.

Tardos et al.[3] applied depletion flocculation mechanism for a long-term physical stability of pesticide concentrates. Pesticide concentrate suspensions form dilatant sediments if they are stored over a period of time. To avoid the formation of dilatant sediment, non-adsorbing polymer can be added to the concentrate dispersion which lead to depletion flocculation and formation of the flocs that can be redispersed easily. Reversible aggregation of red blood cells, of great significance in medicine,[4] is another interesting application.

Depletion flocculation, a thermophysical phenomenon, has been commercially applied to process improvements for colloid dispersion stability in the paint and surface coating industries.[5] This mechanism needs to be formulated further whenever a new system comprising colloid particles, macromolecules and solvent is encountered. An enhanced oil recovery technology that relies in the use of a water-soluble polymer is already being employed for crude oil production in Canada and China.[6] Since crude oil comprises a fraction which is nanoparticulate, it is important to account for the effect of depletion flocculation on reservoir phase and flow behavior.

Commercial simulators cannot predict accurately the phase behavior of mixtures of crude oil + water soluble polymer.

1.2   Flocculation of a Colloid Dispersion by Adding Polymer

Addition of polymer into a colloidal dispersion of nanoparticles and solvent may lead to flocculation or steric stabilization of the dispersion.[7] Flocculation is caused by two mechanisms – depletion flocculation and bridging flocculation. Depletion flocculation occurs when a non-adsorbing polymer is used as a flocculating agent, while bridging flocculation occurs when polymer molecules adsorb on the surface of more than one nanoparticle. The two mechanisms are shown in Figure 1.1. Over time, the dispersions separate into two phases. The kinetics of separation and the compositions of the phases depends on the nature of the interaction between polymer coils and nanoparticles. For non-adsorbing polymers, the phase separation leads to a solvent + polymer rich phase and a solvent + particle rich phase. For adsorbing polymers, phase separation results in a polymer + particle rich phase and a solvent rich phase.

The bridging flocculation mechanism is readily visualized. The depletion flocculation mechanism requires more detailed explanation. Asakura & Oosawa[8] explained the depletion flocculation mechanism by treating both the particles and the non-adsorbing polymer molecules as hard spheres. Their simplified model is illustrated in Figure 1.2 and elaborated below.
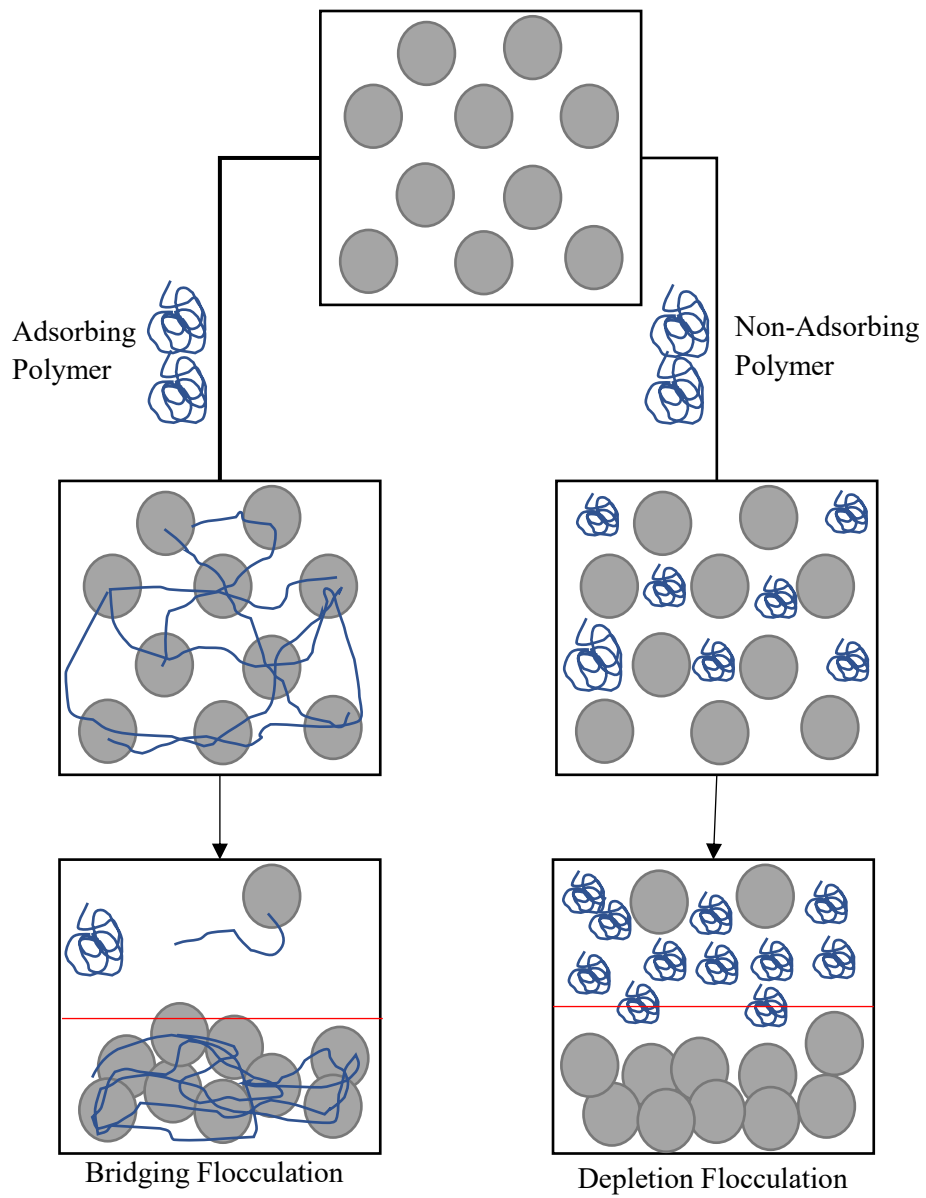
Figure 1.1. Particle flocculation driven by depletion and bridging flocculation mechanisms

Adsorbing Polymer

Non-Adsorbing Polymer

Bridging Flocculation

Depletion Flocculation
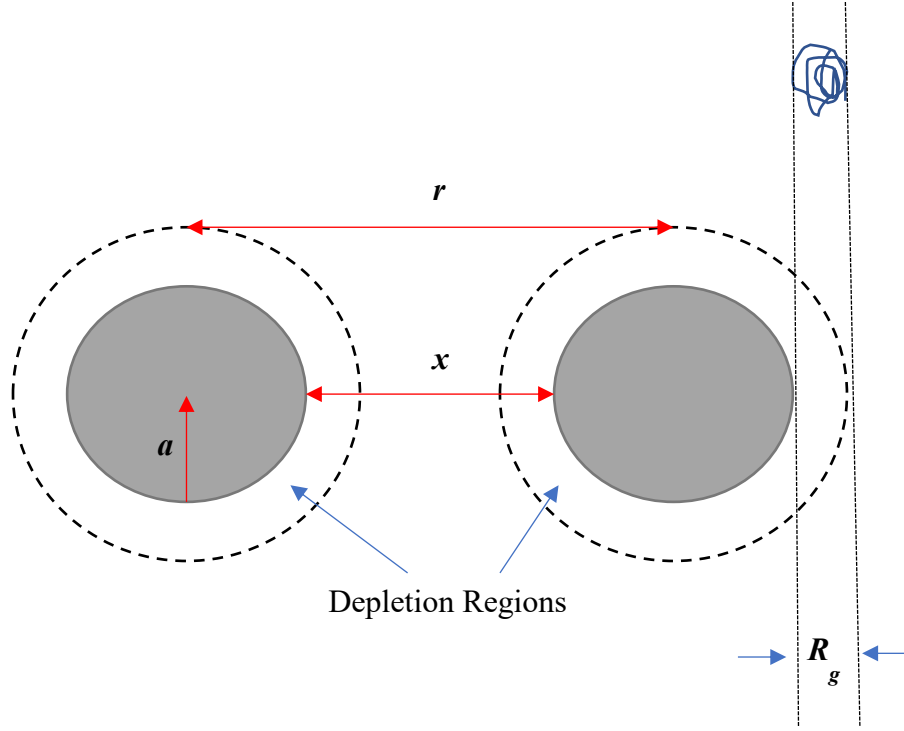
Figure 1.2. Asakura-Oosawa free volume theory model for the depletion flocculation mechanism. a, particle size; R_g, radius of gyration of polymer coil; r, radial distance between centers of two particles and x, radial distance between two particles surfaces.

In the Asakura-Oosawa model the Gibbs energy for depletion flocculation, $G_{Depletion}$, is defined as:

$$G_{Depletion} = \Delta p . \Delta V \qquad (1\text{-}1)$$

where ΔV is the free volume available to polymer coils as a result of overlapping depletion zones and Δp is the osmotic pressure difference between depleted zone and bulk. ΔV can be calculated using the equation reported by Jenkins et al.,[7]:

$$\text{for } 2a < x < 2\,a + 2\,R_g, \quad \Delta V = \frac{4}{3}\pi \left(a + R_g\right)^3 \left(1 - \frac{3r}{4(a+R_g)} + \frac{r^3}{16(a+R_g)^3}\right) \qquad (1\text{-}2)$$

4

for $\qquad x > 2\,a + 2\,R_g,\qquad \Delta V = 0$ (1-3)

The variables in equations 1-2 & 1-3:

a	the average radius of particles in a colloid dispersion
R_g	the average radius of gyration of polymer coils
r	the average central distance between two particles

and are defined in the nomenclature along with other variables used in the thesis.

Osmotic pressure, Δp is given by:

$$\Delta p = -\rho_{polymer}(kT)$$ (1-4)

where $\rho_{polymer}$ is the density of non-adsorbing polymer in bulk and kT is the Boltzmann thermal energy. By combining expressions (1-1), (1-2) and (1-4) an expression for depletion Gibbs energy is obtained:

for $2a < x < 2\,a + 2\,R_g$,

$$G_{Depletion} = -\frac{4}{3}\pi\left(a + R_g\right)^3\left(1 - \frac{3r}{4(a+R_g)} + \frac{r^3}{16(a+R_g)^3}\right)\rho_{polymer}(kT)$$ (1-5)

This conceptually simple expression for Gibbs energy of depletion flocculation is not accurate at high polymer concentration, but provides insights into the phase behaviors associated with depletion flocculation.

1.3   Molecular Liquid-Liquid Phase Behaviors for Polymer + Solvent Mixtures

Polymers in a solvent generally exhibit an UCEP temperature and display liquid-liquid phase behavior at lower temperatures.[9] At temperatures well above UCEP, the solvent is a so-called good solvent for the polymer (present in coil form)[10]. Under these conditions the solvent and

polymer are miscible, as shown in Figure 1.3. At temperatures below the UCEP temperature, the polymer (present in globule form)[10] and the solvent are not miscible. Polymer rich and solvent rich phases coexist. This behavior is entropically driven. At these conditions polymer-polymer interaction is preferred over polymer-solvent interaction.

| T > UCEP | T = UCEP | T < UCEP |
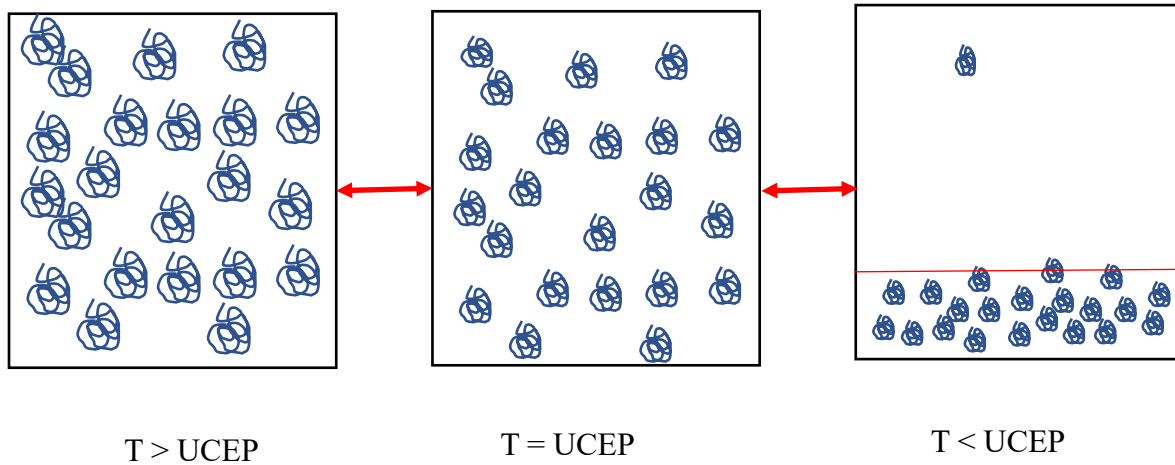
Figure 1.3. Phase behavior of a polymer + solvent mixture above and below the UCEP temperature.

Sanchez and Lacombe[11] formulated the Gibbs free energy of a pure polymer + pure solvent mixture. Their model is based on a lattice where n_1 (solvent molecules) were mixed with n_2 (polymer chains). The Gibbs energy of mixing is given by:

$$\Delta G^{mixing} = \Delta H^{mixing} - T\Delta S^{mixing} \tag{1-6}$$

where ΔH^{mixing} - the enthalpy of mixing and ΔS^{mixing} - the entropy of mixing, is based on combinatorics and given by:

$$\Delta S^{mixing} = -k(n_1\emptyset_1 + n_2\emptyset_2) \tag{1-7}$$

where $\varnothing_1$ and $\varnothing_2$ are the partial molar volume of polymer and solvent respectively in a polymer solution. The enthalpy of mixing, assuming that only the interaction between polymer segments and solvent molecules contributes, given by:

$$\Delta H^{mixing} = n_1\varnothing_2 X_{1-2}kT \tag{1-8}$$

where $X_{1-2}kT$ is the energy difference between a state comprising only solvent and a state comprising solvent + pure polymer. X_{1-2} is an interaction parameter. By combining expression (1-6) to (1-8), the Gibbs energy of mixing of a polymer + solvent mixture becomes:

$$\Delta G^{mixing} = n_1\varnothing_2 X_{1-2}kT + (n_1\varnothing_1 + n_2\varnothing_2)kT \tag{1-9}$$

Equation 1-9 provides insights into the temperature dependent liquid-liquid phase behavior of polymer + solvent mixtures.

In this work, interactions between phase diagram arising from depletion flocculation, Figure 1.1, and polymer-solvent liquid-liquid phase behavior, Figure 1.3 are explored based on the behavior of the ternary mixture polystyrene + cyclohexane + silica nanoparticles. Key features of the polystyrene + cyclohexane binary phase diagram, a well-studied mixture, are rehearsed, and provide an experimental reference mixture. The polystyrene + silica nanoparticle and cyclohexane + silica nanoparticles binaries are assumed to be uniform colloids.

1.4   Thesis Motivation and Overview

The surface and molecular interaction between polymers, nanoparticles and solvent molecules is important for industrial and environmental applications ranging from pharmaceutical formulation to tackling the behavior of fine clays in tailings ponds. While depletion flocculation driven phase behavior and polymer + solvent phase behavior has been studied individually, the interaction between these two types of phase behavior and near the UCEP temperature of the polymer + solvent binary mixture in particular has received little attention in the open literature. From this exploratory work, new types of phase diagrams comprising enabling technologies for separation and formulation are anticipated.

This thesis is divided in five chapters, including this overview. The remaining chapters are:

Chapter 2- Literature reviews of the phase behaviours of polymer + solvent binary mixtures, the depletion flocculation effect and the phase diagrams of non-absorbing polymers and colloid particles in solvents are presented.

Chapter 3- Experimental aspects of the research are provided. The phase behavior visualization apparatus, an X-ray view cell, is described and discussed. Sample preparation and experimental procedures including quantitative temperature measurement and image processing, and result uncertainty and validation are addressed.

Chapter 4- Experimental results including (co-existing phase compositions, critical phenomena, and phase diagrams) are presented and discussed. Implications and potential applications are described.

Chapter 5- The conclusions and future work arising from this study are presented.

1.5   Nomenclature

a	particle size
R_g	radius of gyration of polymer coil
r	radial distance between centers of two particles and
x	radial distance between two particles surfaces
$G_{Depletion}$	Gibbs energy for depletion flocculation
ΔV	depletion free volume
Δp	osmotic pressure difference
kT	Boltzmann thermal energy
UCEP	upper critical end point
ΔG^{mixing}	Gibbs energy of mixing
ΔH^{mixing}	enthalpy of mixing
ΔS^{mixing}	entropy of mixing
$\emptyset_1$	partial volume fraction of polymer
$\emptyset_2$	partial volume fraction of solvent
n_1	number of solvent molecules
n_2	number of polymer chains
X_{1-2}	interaction parameter

1.6   References

1.   Lekkerkerker, H.; Poon, W.; Pusey, P. N.; Stroobants, A.; Warren, P. 0. Phase behaviour of colloid polymer mixtures. EPL (Europhysics Letters) **1992**, 20, 559.

2.   Fleer, G. J.; Tuinier, R. Analytical phase diagrams for colloids and non-adsorbing polymer. Adv. Colloid Interface Sci. **2008**, 143, 1-47.

3.   Tadros, T. F.; Zsednai, A. Application of depletion flocculation for prevention of formation of dilatant sediments. Colloids and Surfaces **1990**, 43, 105-116.

4.   Chien, S.; Simchon, S.; Abbott, R. E.; Jan, K. Surface adsorption of dextrans on human red cell membrane. J. Colloid Interface Sci. **1977**, 62, 461-470.

5.   Stahl, G. A.; Schulz, D. N. Water-soluble polymers for petroleum recovery; Springer Science & Business Media: **2012**; .

6.   Ogden, A. L.; Lewis, J. A. Effect of nonadsorbed polymer on the stability of weakly flocculated suspensions. Langmuir **1996**, 12, 3413-3424.

7.   Jenkins, P.; Snowden, M. Depletion flocculation in colloidal dispersions. Adv. Colloid Interface Sci. **1996**, 68, 57-96.

8.   Asakura, S.; Oosawa, F. On interaction between two bodies immersed in a solution of macromolecules. J. Chem. Phys. **1954**, 22, 1255-1256.

9.   Koningsveld, R.; Kleintjens, L. A. Liquid-liquid phase separation in multicomponent polymer systems. X. Concentration dependence of the pair-interaction parameter in the system cyclohexane-polystyrene. Macromolecules **1971**, 4, 637-641.

10.   Sun, S.; Nishio, I.; Swislow, G.; Tanaka, T. The coil–globule transition: radius of gyration of polystyrene in cyclohexane. J. Chem. Phys. **1980**, 73, 5971-5975.

11.   Sanchez, I. C.; Lacombe, R. H. Statistical thermodynamics of polymer solutions. Macromolecules **1978**, 11, 1145-1156.

Chapter 2. Literature Review

2.1   Introduction to Colloidal Dispersions and Key Terminology

Colloidal dispersions comprise a dispersed phase and a continuous medium, where one of the dimensions of the particles, drops or bubbles of the dispersed phase is in range of 10^{-9} m to 10^{-6} m.[1] This review focuses on colloid suspensions where the dispersed phase comprises solid particles and the surrounding medium is a single-phase liquid. Mixtures where both of the dispersed phase and continuous medium are liquids are also addressed.

2.1.1   Lyophilic and Lyophobic Colloid Suspensions

Lyophilic colloids, comprise solid particles uniformly and stably distributed in a solvent in the absence of any thermophysical or chemical change. Lyophobic colloids settle over time in the absence of agitation, resulting in a phase separation, known as "surface generation" between the continuous and dispersed phases.[1]   Flocculation can also take place in lyophobic colloidal dispersions. Particles can floc in response to thermophysical change or agitation. Flocculation facilitates separation.

2.1.2   Macromolecular and Nano Colloids

Macromolecular colloids for example polystyrene, a non-adsorbing polymer (dispersed phase) in cyclohexane (continuous medium), and Nano colloid, silica nanoparticles (dispersed phase) in cyclohexane (continuous medium), are two different classes of colloid suspension. The polymer coils or macromolecules in a dispersion can transform shape in response to thermophysical or

chemical changes, while the nanoparticles remain rigid - though can form aggregates and flocculate in a dispersion.

Colloid particles behave like an ideal gas in a non-interacting environment i.e., if there is no attraction or repulsion between particles and solvent molecules. Generally, in a colloid suspension, interparticle forces lead to aggregates or flocs, and other phenomena that underlie the field of Colloidal Chemistry.

2.1.3 Polydispersity and Molar Mass Averages

All colloidal dispersions are nominally poly dispersed. If the size distribution is narrow, they may be approximated as mono dispersed. In this work, the number average diameter, $\overline{d}$, of solid particles is defined as:

$$\overline{d} = \frac{\sum_i n_i d_i}{\sum_i n_i}$$

(2-1)

where, d_i is the diameter of the ith particle class, n_i is the number of particles of a class i, and $\sum_i n_i$ is the total number of particles in a colloid dispersion. The standard deviation, σ, for the particle size distribution is:

$$\sigma = \frac{\sum_i n_i (d_i - \overline{d})^2}{\sum_i n_i - 1}$$

(2-2)

The number average molar mass for polymers, $\overline{M}_n$ comprising n molecules where the molar mass of the ith class of molecules is M_i, is given by:

$$\overline{M}_n = \frac{\sum_i n_i M_i}{\sum_i n_i}$$

(2-3)

Similarly, the mass average molar mass, $\overline{M}_w$ is given by:

$$\overline{M}_w = \frac{\Sigma_i w_i M_i}{\Sigma_i w_i} \tag{2-4}$$

where, w_i is the mass of the ith class of molecules M_i:

$$w_i = \Sigma_i n_i M_i \tag{2-5}$$

Using (2-5), equation (2-4) can be simplified further in terms of n_i given by equation (2-6)

$$\overline{M}_w = \frac{\Sigma_i (n_i M_i) M_i}{\Sigma_i (n_i M_i)} = \frac{\Sigma_i n_i M_i^2}{\Sigma_i n_i M_i} \tag{2-6}$$

Experimental $\overline{M}_n$ values are obtained from osmotic pressure measurements. Light scattering is used to measure $\overline{M}_w$.[1] for poly dispersed polymers

$$\frac{\overline{M}_w}{\overline{M}_n} \geq 1 \tag{2-7}$$

and the ratio $\dfrac{\overline{M}_w}{\overline{M}_n}$ is a measure of polymer polydispersity.

2.1.4 Radius of Gyration (R_g)

Radius of gyration and hydrodynamic radius, measured using light scattering,[1] are used to define the size of macromolecules in liquids. If macromolecules are considered as a distribution of discrete volume elements with a mass, m_i then the moment of inertia, I about the axis of rotation of the body is given by:

$$I = \sum_i m_i r_i^2 \tag{2-8}$$

where r_i is the position of ith element from the axis of rotation. The radius of gyration is defined as the distance from the axis of rotation of the particle distribution where the entire mass of the system can be allocated thus, the moment of inertia about the axis remains the same.

$$R_g^2 \sum_i m_i = I = \sum_i m_i r_i^2 \tag{2-9}$$

$$R_g^2 = \frac{\sum_i m_i r_i^2}{\sum_i m_i} \tag{2-10}$$

Light scattering measurements[1] give the values of R_g independently of the particle shape. Sometimes the hydrodynamic radius, R_h is reported. It is obtained from the diffusion coefficients of a polymer in solution also from light scattering experiments. A relationship between radius of gyration and hydrodynamic radius is provided by Kok and Rudin[2]:

$$R_h = 0.77 R_g \tag{2-11}$$

2.2   Polymer + Solvent Binary Phase Diagram

Thermophysical properties and phase behaviours of macromolecules in solvents are important topics in diverse fields of application. Gençaslan et al.,[3] showed that a number of such mixtures exhibit Type II and Type IV global phase behaviour according to the Van Konynenburg and Scott[4] classification scheme for binary mixtures. The generalized pressure-temperature projection for these binary classifications are illustrated in Figure 2.1 (a) and 2.1 (b) respectively. C1 and C2 are L=V critical points for pure components. There are (L1=L2+V) critical end points at lower temperatures, one such point for TYPE II and two such points for TYPE IV phase behaviour. There is one (L1=V+L2) end point at high temperature for Type IV phase behaviour. The transition from LLV to LV and L1=L2+V critical point behaviour at low temperatures, which arise in both phase diagram types, are the focus of the current study. This is because polymers often pyrolyze at high temperatures and the focus is on projections surrounding (L1=L2+V) three-phase critical points – Figure 2.2.[5]
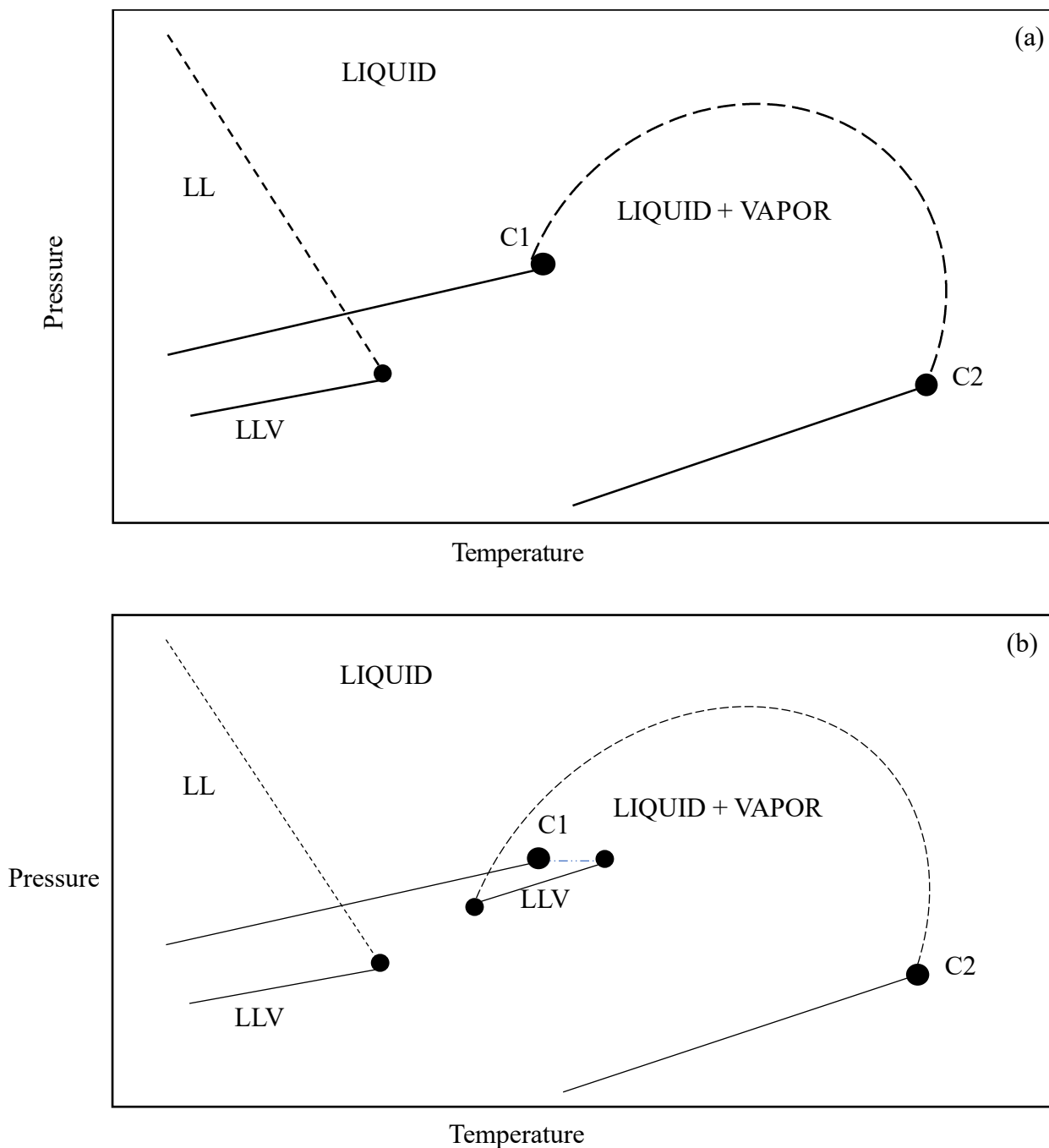
Figure 2.1. Type II (a) and Type IV (b) phase diagrams for binary mixtures. C1 and C2 are critical points for solvent and solute respectively.[4] LL represents a liquid-liquid region LLV represents a liquid-liquid-vapor curve. The dashed curves are critical loci (L1=L2) at low temperature, and L2=V, L1 = V or L1=L2, depending on composition at high temperature.
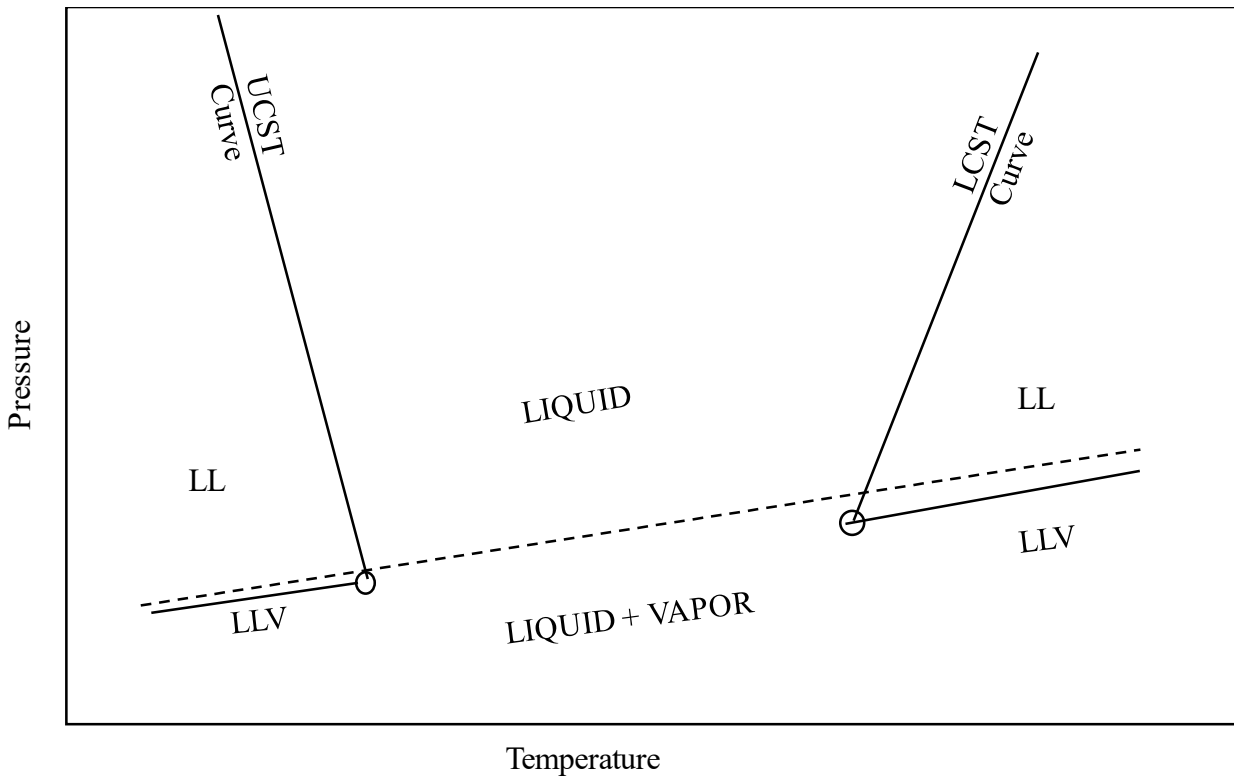
Figure 2.2. Low temperature projection for a polymer + solvent mixture.[5] The UCEP locus (L1=L2 locus) defines the upper temperature limit of the low temperature LL region and is present in both Type II and Type IV binaries. The lower critical end point (LCST) locus (L1=L2 locus) defines the lower temperature bound of the high temperature LL region present in Type IV binary phase diagrams. The dashed line is the vapor pressure of the curve of the solvent.

2.2.1 Liquid-Liquid to Liquid transitions (Cloud Point Curves) for Polystyrene and Cyclohexane Binary Mixtures

The phase behaviour of polystyrene and cyclohexane mixtures is well known. The UCST curve shifts to higher temperature values with increasing polystyrene molar mass, while the LCST curve shifts to lower temperature values concurrently.[6] This work focuses on polymer molar mass of ~ 237 kg/mol and the evaluation of UCSTs (L1=L2 +V) critical points and cloud points (Liquid-liquid to liquid transitions) near room temperature. These transitions are also sensitive to polymer properties, as shown in Figure 2.3.[7-10] Table 2.1 lists the UCEP temperature and composition for four different molar weights of polystyrene in cyclohexane. This combination of properties facilitates experimental design, hypothesis testing and measurement method validation and is the reason polystyrene + cyclohexane mixtures were chosen as a basis for this study.

Table 2.1. UCEP temperature and composition as a function of polystyrene molar weights in polystyrene + cyclohexane binary mixture

Molecular Weight (kg/mol)	UCEP (K) $\pm$ 0.5	UCEP Composition $\pm$ 0.01
45.3	287.7	0.09
103	293.5	0.07
200	297	0.05
498	300.7	0.04
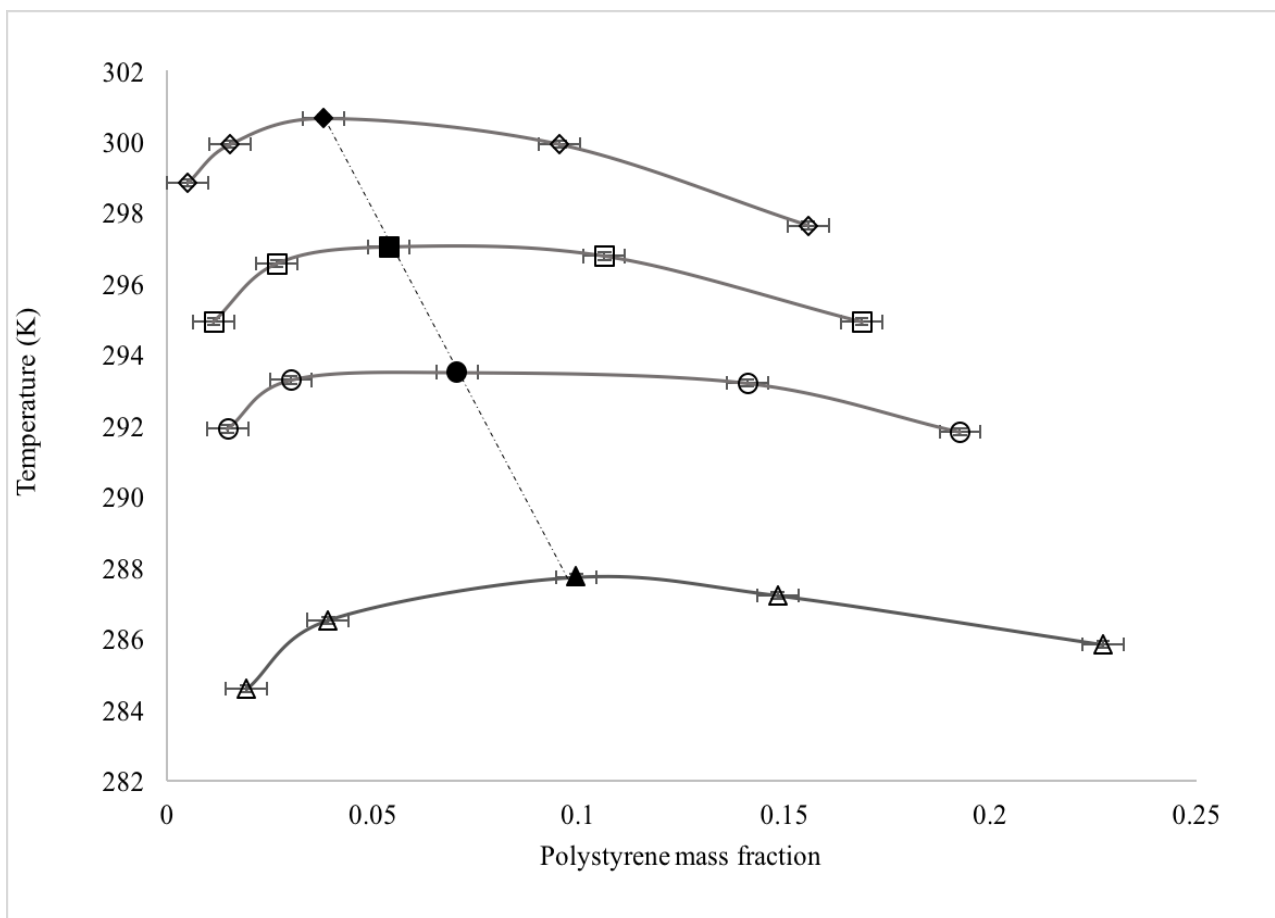
Figure 2.3. Cloud point (L1L2 to L1 and L1L2 to L2 phase transitions) and UCEP data for mixtures of cyclohexane + polystyrene[7-10] mixtures. Symbols represent polystyrene molar mass: ($\diamondsuit$) 498 kg/mol, ($\square$) 200 kg/mol, ($\bigcirc$) 103 kg/mol and ($\triangle$) 45.3 kg/mol. A dotted curve traces the trajectory of UCEP points.

2.2.2 Coil to Globule Transition for Polymers

When polymer coils act as ideal chains in a solvent, the solvent is called a theta (θ) solvent.[11,12] In a good or θ solvent, the interaction between polymer coils and solvent molecules is entropically favourable and the mixture is miscible. In a non θ solvent, polymers form globules and polymer-polymer interaction leads to phase separation. For polystyrene in cyclohexane,

the θ condition is satisfied above the UCST. At any concentration of polystyrene in cyclohexane, there is a transition from coil form to globule or collapsed form at the cloud point as shown in Figure 2.4. The radius of gyration and the hydrodynamic radius decrease significantly as this transition occurs.[13,14]
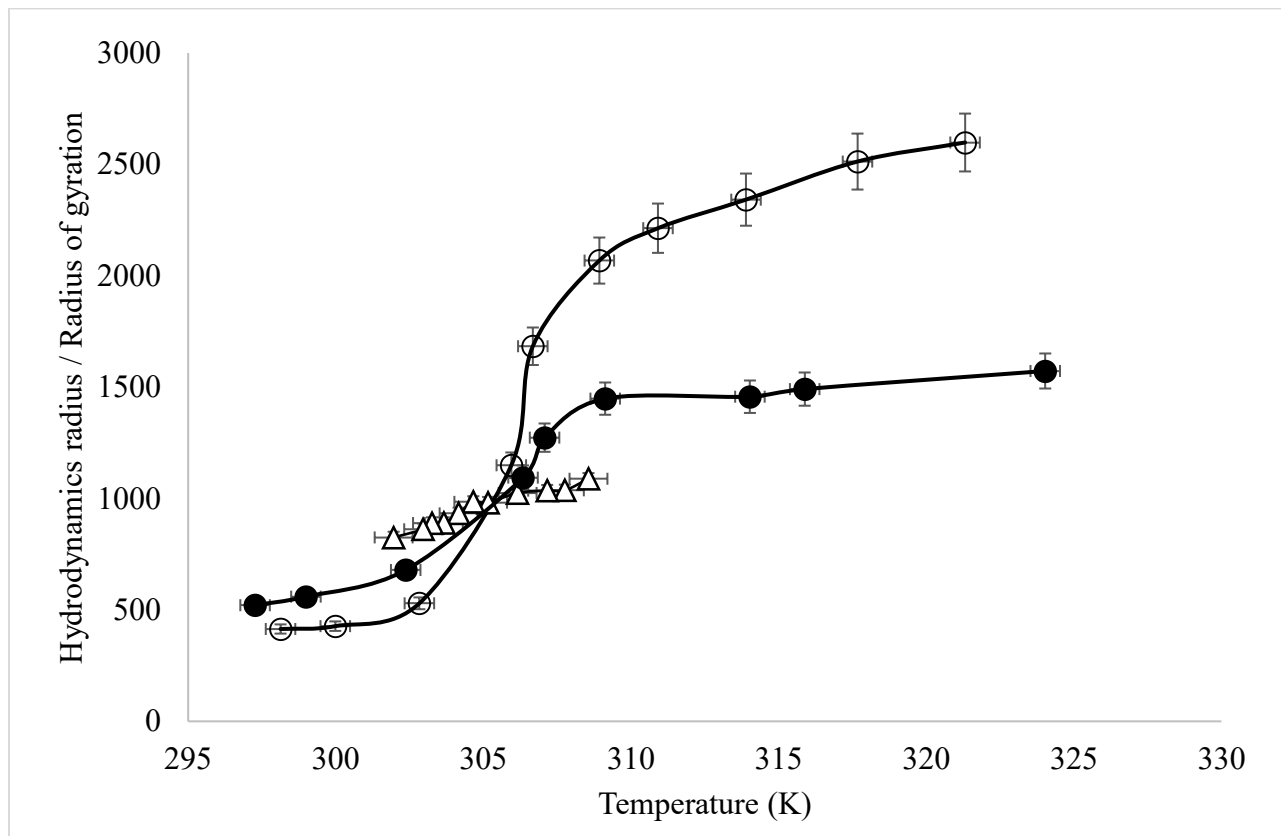
Figure 2.4. Radius of gyration and hydrodynamic radius for polystyrene in cyclohexane near coil-globule transitions.[13,14] Symbols: (●) radius of gyration and (○) hydrodynamic radius for polystyrene molar weight 26000 kg/mol, (△) radius of gyration for polystyrene molar weight 20600 kg/mol.

There are a number of correlations for the radius of gyration and the hydraulic radius of polystyrene in solvents[13-15]. Correlations[15] for radius of gyration and the hydraulic radius for polystyrene in cyclohexane valid for polymer molar masses, *MW* from 10^4 to 10^7 g/mol (used in the present work):

$$R_g = 2.42 * 10^{-2}(MW)^{0.512} \qquad (2\text{-}12)$$

$$R_h = 2.15 * 10^{-2}(MW)^{0.502} \qquad (2\text{-}13)$$

2.3 Polymer + Colloid Mixture Phase Diagrams

When non-adsorbing polymer is added to a colloid dispersion, depletion flocculation can occur. This mechanism for phase separation was introduced by Asakura and Oosawa[16] in 1954 and later discussed by Virj[17] and others. Depletion flocculation is an entropy driven process leading to mixture separation into polymer rich and colloid rich phases at equilibrium. The concepts and basic equations are explained in Chapter 1.

2.3.1 Depletion Flocculation Phase Separation Studies

Emmet and Vincent[18] studied nC_{18} capped silica nanoparticles (size ~ 8.3 nm) + cyclohexane + polydimethylsiloxane (polymer, MW 100 kg/mol) ternary mixture and reported a critical point, at ~ 0.005 volume fraction of polymer and 0.15 volume fraction of nanoparticle, and triple point, at ~ 0.012 volume fraction of polymer and 0.22 volume fraction of nanoparticle. Sperry[19] studied relatively large latex particles (diameter ~ 0.05 to 0.6 μm) with hydroxyethyl cellulose polymer in water and found that the sediment volume fraction due to flocculation increased if either of size of latex particles or polymer concentration were increased in the dispersion. At high polymer concentrations, thermodynamically stable and homogeneous dispersions have been

observed elsewhere for nC$_{18}$ capped silica nanoparticles (size ~ 8.3 nm) + polydimethylsiloxane + cyclohexane and polystyrene capped silica (size ~ 94 to 289 nm) + polystyrene + ethylbenzene.[20,21] The transition to a single-phase homogenous dispersion at high concentration of polymer, is difficult to measure experimentally due to high mixture viscosities. At high polymer molar mass, the upper limit of polymer concentration η' decreases.[22] An empirical correlation[23,24] used to estimate the polymer volume fraction, η' where the transition to a homogenous colloid dispersion occurs, is given by:

$$\eta' = (M_n)^{\mu} \tag{2-13}$$

where M_n is the number average molar mass of the polymer and μ ranges from -0.25 to -0.75. Polymer type and particle radius are exogenous to the correlation. In general, η' decreases with decreasing particle radius, a, as reported elsewhere.[24] Lower polymer volume fraction limits for the depletion flocculation effect to occur also vary with the radius of gyration of the polymer and particle size[20]. De Hek and Virj[23] reported on the ternary polystyrene (MW ~ 8 to 2400 kg/mol) + lyophilic silica (size ~ 21 nm) + cyclohexane. One of their key observations was related to the lower limit polymer concentration, η'', where depletion flocculation is observed. They showed that the limiting polymer volume fraction decreases with increasing polymer molar mass, particle size, a, and particle volume fraction, ϕ.

An understanding of colloid + polymer phase diagrams has been built upon experimental studies, with limited data, backed by statistical work. Phase diagrams at low particle and polymer compositions are available. In this solvent rich composition range phase boundaries are sensitive

to colloid and polymer size. For example, larger particles + low molar mass polymers ($a \gg R_g$) exhibit colloid gas (G), comprising mainly polymer and solvent, and a colloid rich (C) phase comprising mainly particles.[20] Anderson and Lekkerkerker[25] reviewed the experimental and computational work and proposed a general phase diagram, Figure 2.5, relevant for non-adsorbing polymers + nanoparticles + good solvent mixtures where effective size of polymer is larger than the nanoparticles size. In this phase diagram, colloid gas (G), colloid liquid (L) and colloid rich (C) phases arise individually and in combinations with up to three phases in equilibrium simultaneously at fixed temperature and pressure. A phase diagram, relevant for when the polymer (hydraulic radius or radius of gyration) is smaller than the nanoparticle size is shown in (Figure 2.6). This diagram includes a metastable liquid-liquid region, and appears incomplete because it is not clear how GC phase behaviour transitions to LL phase behaviour without other phase behaviours being present.
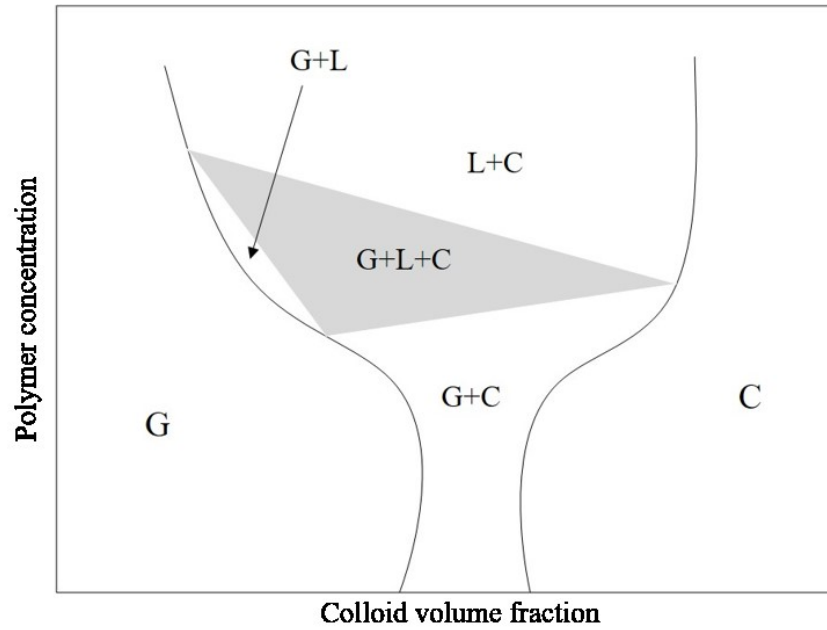
Figure 2.5. An atomic system model showing long range attraction from large polymer with shaded region showing colloid gas (G), liquid (L), and solid (C) like phases in equilibrium.[25]
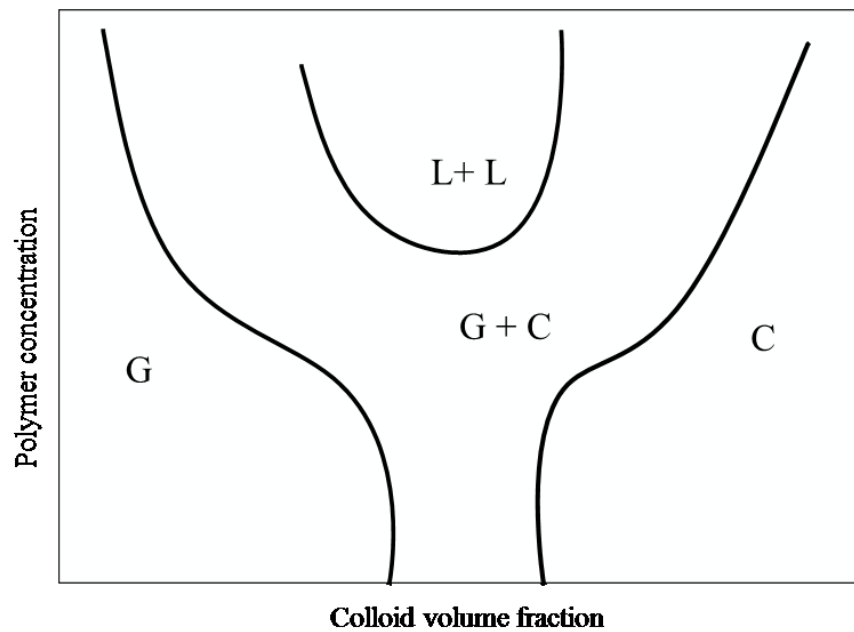
Figure 2.6. Metastable liquid-liquid (L+L) and colloid gas (G) and solid (C) coexistence curve reported in a polymer colloid system.[25]

Theoretical phase diagrams for polymer + colloid mixture that focus on the relationship between radius of gyration of polymer, R_g, and particle radius, a, have been proposed.[26,27] The emergence of a colloid-gas colloid-liquid critical point (G=L) at $\frac{R_g}{a} \sim 0.33$ is an important feature of the phase diagrams reported in Figures 2.7 and 2.8. This feature arises whether the calculations are performed using free volume theory or statistical mechanics.[26-28] At high $\frac{R_g}{a}$ ratios, Figure 2.9, partial phase diagrams include critical phenomena, statistically proven and qualitatively similar to $\frac{R_g}{a} < 1$ shown elsewhere.[29,30]

While phase diagram theory is well developed, experimental phase diagrams are fragmentary and in some cases contradictory. Critical points are frequently not reported. Benchmarking theory with experiment or vice versa is not always feasible.
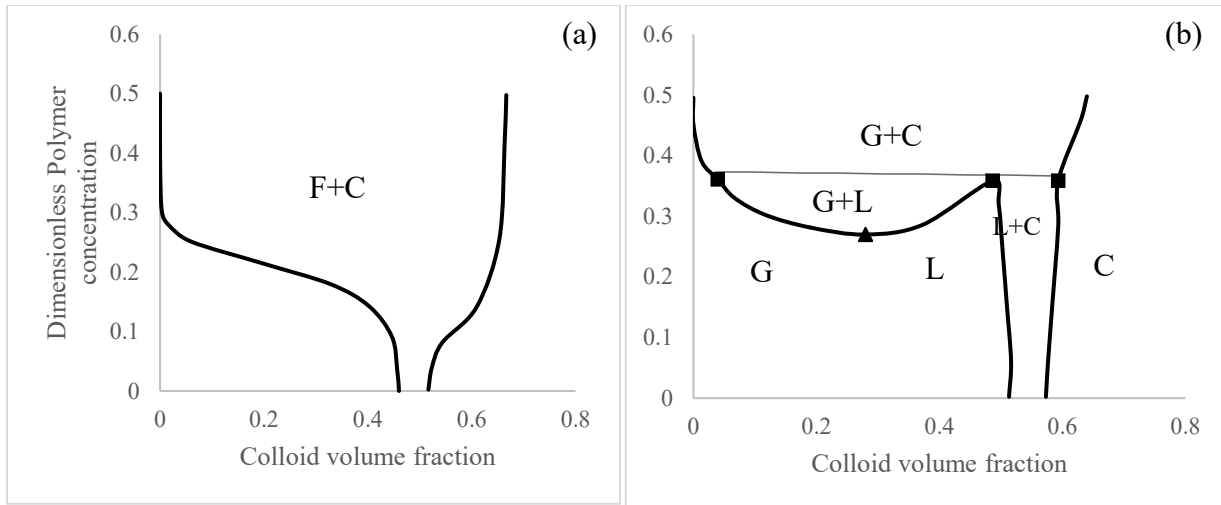
Figure 2.7. Phase diagram of polymer-colloid mixture (statistical mechanics), work by Lekkerkerker et al. [33] for $\frac{R_g}{a} = 0.1$ (a) and $\frac{R_g}{a} = 0.4$ (b). Symbols: (▲) critical point and (■) triple point.
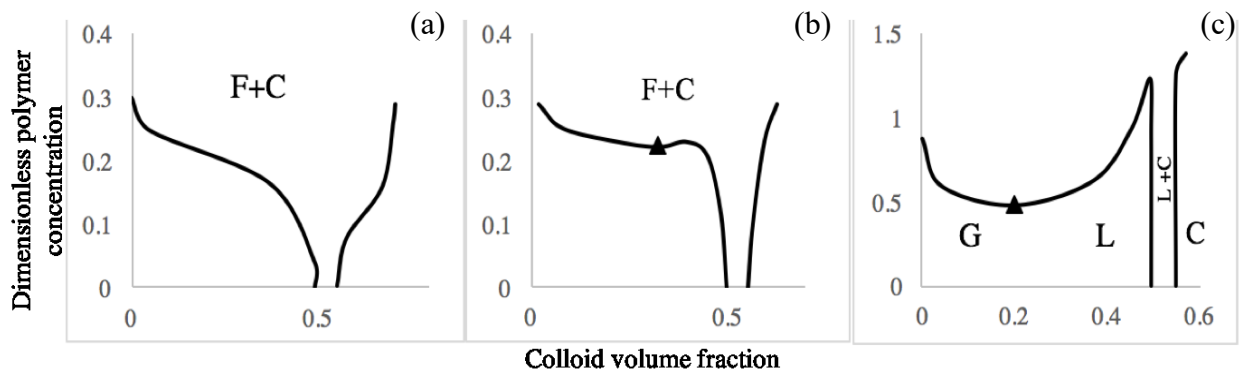
Figure 2.8. Phase diagrams for polymer-colloid mixtures computed using statistical mechanics[34] for $\frac{R_g}{a} = 0.08$ (a), $\frac{R_g}{a} = 0.33$ (b) and $\frac{R_g}{a} = 0.57$ (c). Symbol: (▲) critical point.
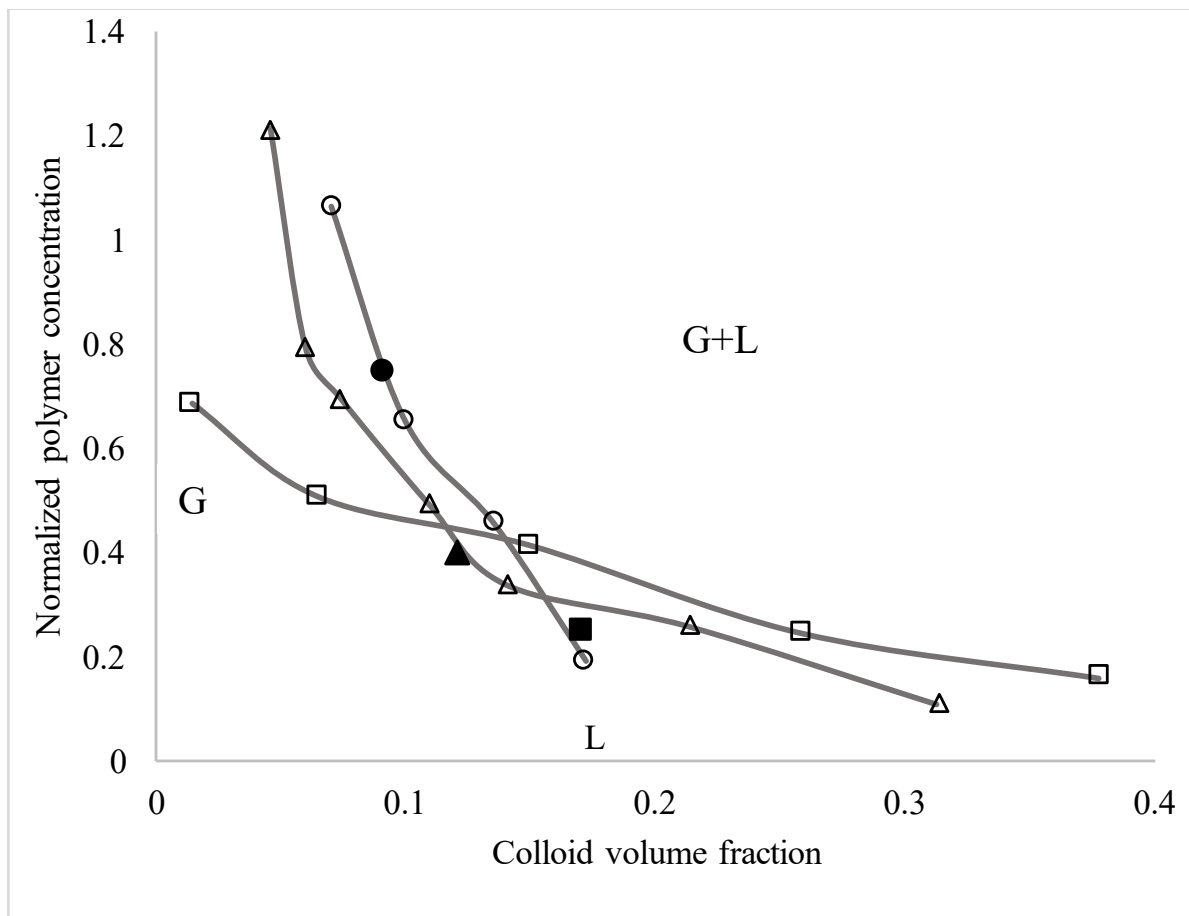
Figure 2.9. Experimental phase diagram for polymer-colloid mixture[29,30] Symbols: ($\bigcirc$) $\frac{R_g}{a}$ =2.2, ($\triangle$) $\frac{R_g}{a}$ =1.4 and ($\square$) $\frac{R_g}{a}$ =0.84. Solid markers represent G=L critical points.[28]

2.3.2   Effect of Temperature on Colloid-Polymer Phase Diagrams

Poon[31] studied the ternary PMMA particles (size ~ 220 nm) + cis-decalin + polystyrene mixtures and observed that phase boundary compositions are sensitive to temperature variation below 286 K (theta temperature) and reported small variation in phase equilibrium conditions near 292 K. Polystyrene globules transition to coils and coils expand with increasing temperature (Figure 2.4). Thus, the polymer to particle size ratio is temperature variant. Above and below the globule

to coil transition temperature, polymer R_g is largely independent of temperature and this effect is expected to be of secondary importance unless the $\frac{R_g}{a}$ ratio is ~ 0.33 where three-phase equilibrium may emerge or be suppressed with temperature variation. For example, polystyrene + toluene + asphaltene mixture[32-34] phase transitions were shown to be temperature independent within experimental uncertainty from 248 K to 298 K – a temperature range below the globule to coil transition for 390 kg/mol mean molar mass polystyrene.

2.4   Nomenclature

$\overline{d}$ average diameter,

d_i diameter of the ith particle class

n_i number of particles of a class i,

$\sum_i n_i$ total number of particles in a colloid dispersion.

σ standard deviation

$\overline{M}_n$ average molar mass comprising n molecules

M_i molar mass of the ith class

$\overline{M}_w$ mass average molar mass

w_i mass of the ith class

R_g radius of Gyration

I moment of inertia

r_i position of ith element from the axis of rotation

R_h hydrodynamic radius

L1   low density liquid phase

L2   high density liquid phase

V   vapor phase

LV   liquid-vapor region

LL	liquid-liquid region
LLV	liquid-liquid-vapor curve
C1/C2	critical points
LCST	lower critical solution temperature
UCST	upper critical solution temperature
UCEP	upper critical end point
L1L2	low density liquid-high density liquid region
θ	theta temperature
MW	molar mass of polymer
η'	upper limit of polymer volume fraction
η''	lower limit of polymer volume fraction
μ	arbitrary constant
a	particle size
ϕ	particle volume fraction
G	colloid gas like phase
L	colloid liquid like phase
C	particle rich phase

G+C   colloid gas-particle region

G+L   colloid gas-liquid region

L+C   colloid liquid-particle region

G+L+C   colloid gas-liquid-particle region

L+L   colloid liquid-liquid region

2.5   References

1.   Hiemenz, P. C.; Rajagopalan, R. Principles of Colloid and Surface Chemistry, revised and expanded; CRC press: **1997**; Vol. 14.

2.   Kok, C. M.; Rudin, A. Relationship between the hydrodynamic radius and the radius of gyration of a polymer in solution. Macromolecular Rapid Communications **1981**, 2, 655-659.

3.   Gençaslan, M.; Bilgin, Y.; Keskin, M. Systematic investigation of the global phase behavior of polymer–solvent systems in the density–density plane. Fluid Phase Equilib. **2011**, 301, 191-199.

4.   Konynenburg, P. H. V.; Scott, R. L. Critical Lines and Phase Equilibria in Binary Van Der Waals Mixtures. Philos. Trans. R. Soc. Lond. A **1980**, 298, 495.

5.   McHugh, M.; Krukonis, V. Supercritical fluid extraction: principles and practice; Elsevier: **2013**.

6.   Saeki, S.; Kuwahara, N.; Konno, S.; Kaneko', M. Upper and Lower Critical Solution Temperatures in Polystyrene Solutions. Macromolecules **1973**, 6, 246-250.

7.   Terao, K.; Okumoto, M.; Nakamura, Y.; Norisuye, T.; Teramoto, A. Light-scattering and phase-separation studies on cyclohexane solutions of four-arm star polystyrene. Macromolecules **1998**, 31, 6885-6890.

8.   Tsuyumoto, M.; Einaga, Y.; Fujita, H. Phase equilibrium of the ternary system consisting of two monodisperse polystyrenes and cyclohexane. Polym. J. **1984**, 16, 229-240.

9.   Nakata, M.; Kuwahara, N.; Kaneko, M. Coexistence curve for polystyrene–cyclohexane near the critical point. J. Chem. Phys. **1975**, 62, 4278-4283.

10.   Kamide, K.; Matsuda, S.; Dobashi, T.; Kaneko, M. Cloud point curve and critical point of multicomponent polymer/single solvent system. Polym. J. **1984**, 16, 839-855.

11.   Geschke, D. Physical Properties of Polymers Handbook. Zeitschrift fr Physikalische Chemie **1997**, 199, 128.

12.   Flory, P.; Cherayil, B. Spatial configuration of macromolecular chains. Reson **2003**, 8, 82-90.

13.   Sun, S.; Nishio, I.; Swislow, G.; Tanaka, T. The coil–globule transition: radius of gyration of polystyrene in cyclohexane. J. Chem. Phys. **1980**, 73, 5971-5975.

14.   Vidakovic, P.; Rondelez, F. Temperature dependence of the hydrodynamic radius of flexible coils in solutions. 2. Transition from the θ to the collapsed state. Macromolecules **1984**, 17, 418-425.

15.   Fetters, L. J.; Hadjichristidis, N.; Lindner, J. S.; Mays, J. W. Molecular Weight Dependence of Hydrodynamic and Thermodynamic Properties for Well-Defined Linear Polymers in Solution. J. Phys. Chem. Ref. Data **1994**, 23, 619-640.

16.   Asakura, S.; Oosawa, F. On interaction between two bodies immersed in a solution of macromolecules. J. Chem. Phys. **1954**, 22, 1255-1256.

17.   Vrij, A. Polymers at interfaces and the interactions in colloidal dispersions. Pure Appl. Chem. **1976**, 48, 471-483.

18.   Emmett, S.; Vincent, B. Phase separation in dispersions of weakly interacting particles induced by non-adsorbing polymer. Phase Transitions: A Multinational Journal **1990**, 21, 197-206.

19.   Sperry, P. R. Morphology and mechanism in latex flocculated by volume restriction. J. Colloid Interface Sci. **1984**, 99, 97-108.

20.   Jenkins, P.; Snowden, M. Depletion flocculation in colloidal dispersions. Adv. Colloid Interface Sci. **1996**, 68, 57-96.

21.   Clarke, J.; Vincent, B. Nonaqueous silica dispersions stabilized by terminally anchored polystyrene: The effect of added polymer. J. Colloid Interface Sci. **1981**, 82, 208-216.

22.   Vincent, B.; Edwards, J.; Emmett, S.; Jones, A. Depletion flocculation in dispersions of sterically-stabilised particles ("soft spheres"). Colloids and Surfaces **1986**, 18, 261-281.

23.   De Hek, H.; Vrij, A. Phase separation in non-aqueous dispersions containing polymer molecules and colloidal spheres. J. Colloid Interface Sci. **1979**, 70, 592-594.

24.   Vincent, B.; Edwards, J.; Emmett, S.; Croot, R. Phase separation in dispersions of weakly-interacting particles in solutions of non-adsorbing polymer. Colloids and Surfaces **1988**, 31, 267-298.

25.   Anderson, V. J.; Lekkerkerker, H. N. Insights into phase transition kinetics from colloid science. Nature **2002**, 416, 811-815.

26.   Lekkerkerker, H.; Poon, W.; Pusey, P. N.; Stroobants, A.; Warren, P. 0. Phase behaviour of colloid polymer mixtures. EPL (Europhysics Letters) **1992**, 20, 559.

27.   Ilett, S. M.; Orrock, A.; Poon, W.; Pusey, P. N. Phase behavior of a model colloid-polymer mixture. Physical Review E **1995**, 51, 1344.

28.   Fleer, G. J.; Tuinier, R. Analytical phase diagrams for colloids and non-adsorbing polymer. Adv. Colloid Interface Sci. **2008**, 143, 1-47.

29.   Ramakrishnan, S.; Fuchs, M.; Schweizer, K. S.; Zukoski, C. F. Entropy driven phase transitions in colloid–polymer suspensions: Tests of depletion theories. J. Chem. Phys. **2002**, 116, 2201-2212.

30.   Lynch, I.; Cornen, S.; Piculell, L. Investigation of the segregative phase separation induced by addition of polystyrene to AOT oil-continuous microemulsions. J. Phys. Chem. B **2004**, 108, 5443-5452.

31.   Poon, W. The physics of a model colloid–polymer mixture. J. Phys.: Condens. Matter **2002**, 14, R859.

32.   Khammar, M.; Shaw, J. M. Liquid-Liquid Phase Equilibria in Asphaltene + Polystyrene + Toluene Mixtures at 293 K, Energy & Fuels **2012**, 26(2), 1075-1088.

33.   Khammar, M.; Shaw, J. M. Estimation of Phase Composition and Size of Asphaltene Colloidal Particles in Mixtures of Asphaltene + Polystyrene + Toluene at 293 K and Atmospheric Pressure. Fluid Phase Equilibria **2012**, 332, 105-119.

34.   Pouralhosseini, S.; Shaw, J. M. Temperature-Independent Colloidal Phase Behavior of Maya Asphaltene + Toluene + Polystyrene Mixtures. Energy & Fuels **2015**, 29(8), 4864-4873.

Chapter 3. Experimental

3.1   Materials

Cyclohexane, high pressure liquid chromatography (HPLC) grade, n-heptane, 0.2 micron filtered and, toluene, HPLC grade, were obtained from Fisher Scientific and their % assay, refractive index (RI), density at 298 K and maximum water impurity are provided in Table 3.1. These compounds were used as received.

Table 3.2. List of organic solvents used and their properties

Solvent	% Assay	RI at 298 K	Density at 298 K (g/mL)	Water impurity (ppm)
Toluene	99.90	1.424	0.772	5
n-Heptane (C_7)	99.60	1.385	0.684	3
Cyclohexane	99.99	1.495	0.779	2

Atactic, isotactic and syndiotactic forms of polystyrene are shown in Figure 3.1. The atactic form, has aromatic rings randomly distributed on both sides of the polymer backbone[1]. The syndiotactic form is highly regular and crystalline while the atactic form is amorphous due to the random stereo-chemical structure. Atactic Polystyrene beads, with a mass average molar mass (MW) of 237 kg/mol, were obtained from Alfa Aesar. The number average molar mass (Mn) approximately equals the MW with polydispersity less than 1.06.

Fumed silicon dioxide (silica) nanoparticles (NPs) were purchased from Sigma Aldrich. The particles have an average diameter of 7 nm and an intrinsic density of 2.3 g/mL at 298 K. The

NPs have a reported surface area of 395 ± 25 m^2/g, melting point of 2473 K at atmospheric pressure, and pH in the range of 3.6 – 4.3. Particles are non-porous, amorphous and hygroscopic.
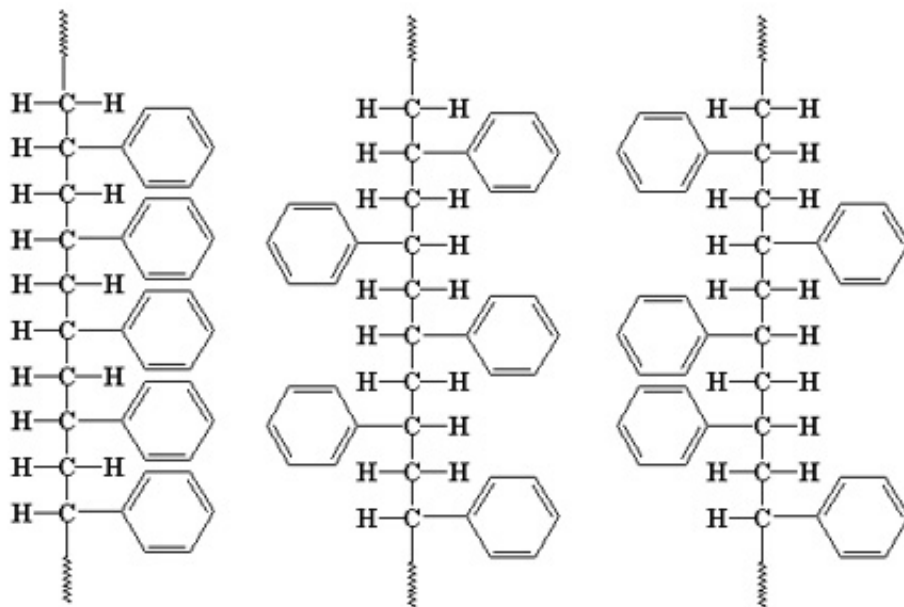
Figure 3.1. Forms of Polystyrene: isotactic (left), syndiotactic (middle) and atactic (right).

3.2 Cloud Point Measurements

Cloud points for cyclohexane + polystyrene mixtures have been reported.[2-4] In this work, cloud points were measured using the apparatus shown in Figure 3.2. It comprises a glass vial, a stirrer that sits at the bottom of the vial, a water bath, a resistance temperature detector (RTD) connected to a display, a heater/stirrer plate and a video camera. Samples were prepared in the glass vial and inserted in the water bath. The temperature of the bath was increased at ~ 0.4 K/min and monitored with the RTD. Both the bath and the vial were stirred continuously. A video camera was used to record the changes in the turbidity of samples and to record temperatures. The videos were analyzed to identify cloud points. At cloud points, mixtures

transition from two phases to one phase and samples go from turbid to clear. An example is shown in Figure 3.3. Reported cloud point data have an uncertainty of 0.3 K.
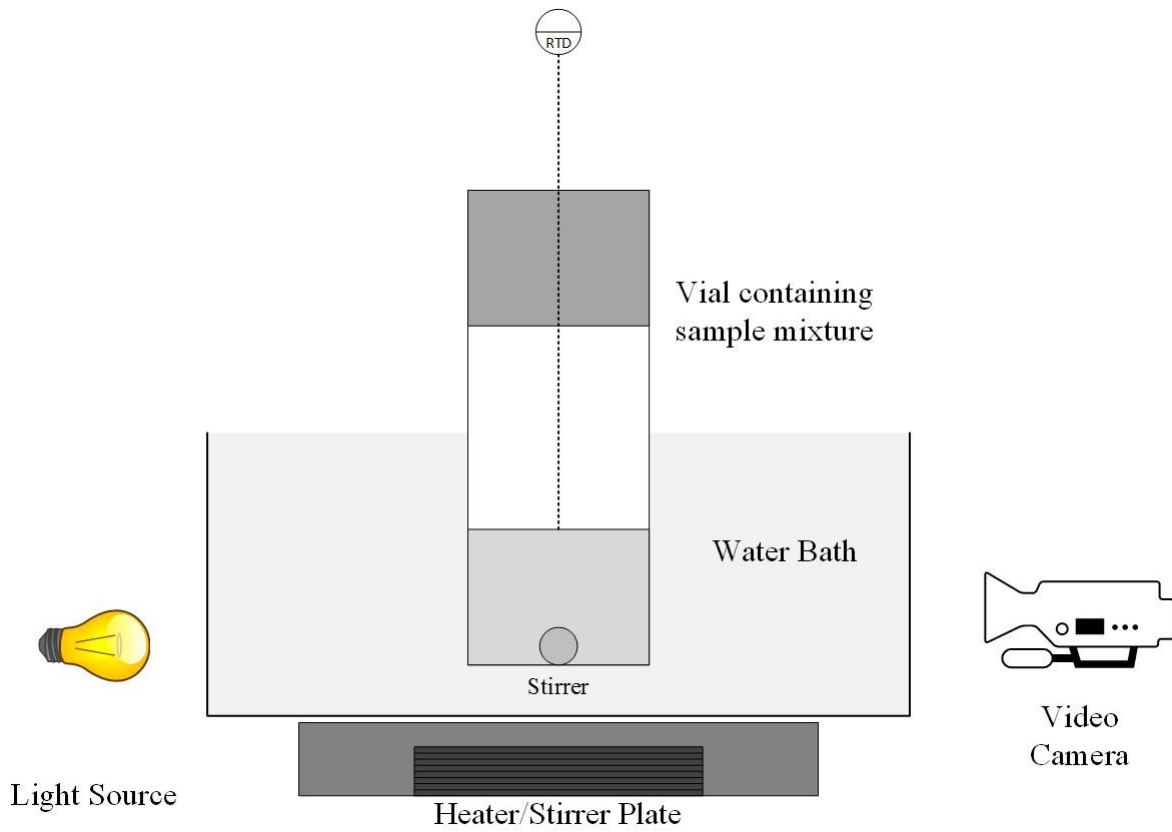
Figure 3.2. A schematic showing setup for cloud point measurements of solid free mixtures.
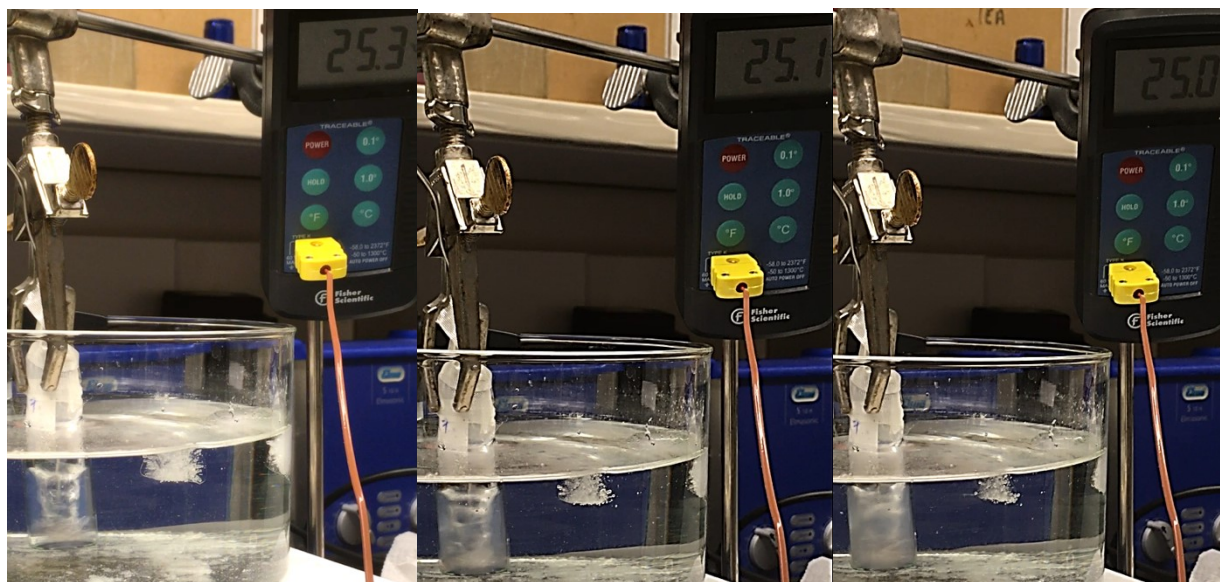
Figure 3.3. Three frames of a video showing the transition from one phase to two phases of the (1:9) polystyrene: cyclohexane control mixture. As the temperature changes from 298.3 K to 298.0 K, the clear mixture turns turbid. (Video link provided in Supplementary Materials on page 94)

3.3   Liquid-Liquid Equilibrium Measurement

The X-ray view cell unit was developed and modified over 20 years and has been used to study the phase behaviour of diverse mixtures at pressures ranging from 0 to 26 MPa and temperatures ranging from 300 K to 700K.[5-9] For this study, the high-pressure cell and custom heating jacket were replaced. Depletion flocculation and liquid-liquid (LL) phase behaviour at atmospheric pressure were observed using calibrated 22 mL glass vials with septa caps. A thermocouple was inserted through the septa. Temperature was increased/decreased within the temperature range 296 K to 338 K (with an uncertainty of $\pm$ 0.2 K) by applying a heat tracing on the glass vial wall and using a one-zone benchtop heater controller provided by Metarock Laboratories. A small stainless steel stirrer inserted in the vial and the magnet motor inside the view cell, were used to

control the mixing. A sketch showing the arrangement of the vial, heating, and stirring elements is shown in Figure 3.4. The X-ray telemetry, the x-ray cabinet and safety interlocks were retained. A polychromatic X-ray beam is transmitted through the view cell and captured by an X-ray image intensifier (Simens 11 and 28 cm dual field cesium iodide). An inline video camera (Pulnix tm-9710) processes intensity into black and white digital images using a 256-point gray scale. The images are monitored on a computer. A schematic of the equipment is shown in Figure 3.5.
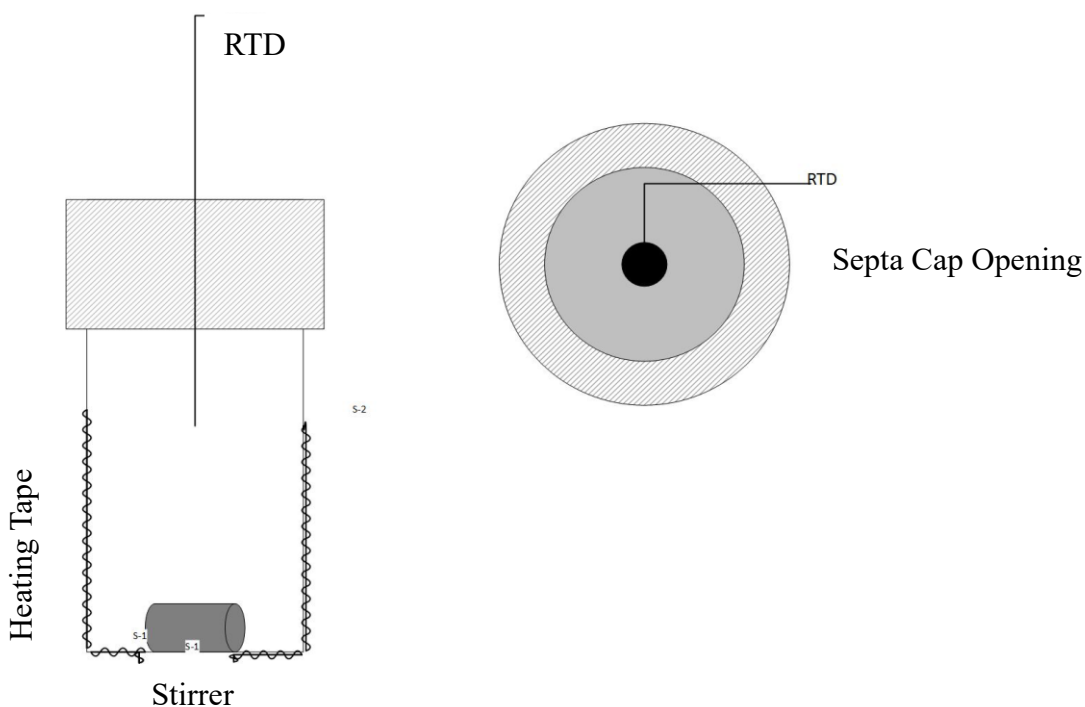
Figure 3.4. View cell detail.
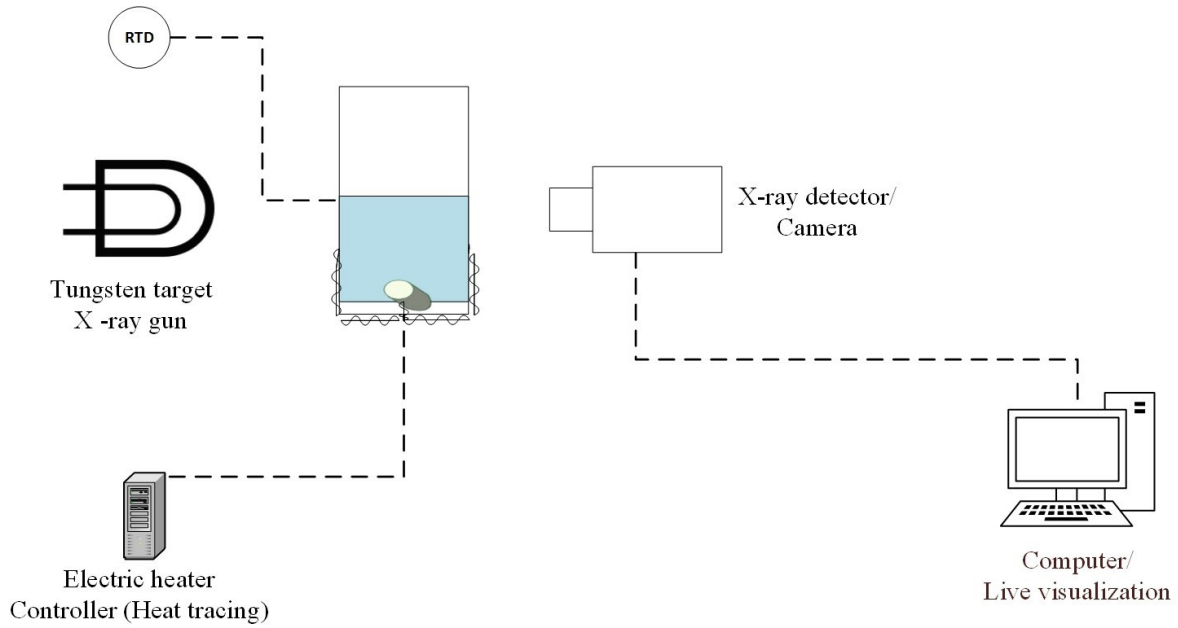
Figure 3.5. Schematic of the x-ray view cell set up.

3.4.1 X-ray tomography physics

The polychromatic X- ray beam with intensity, I_o passes through the sample and the transmitted beam of intensity, I is recorded using an image intensifier in the form of two dimensional values of shades of gray. The incident beam losses energy accounting to photoelectric adsorption and scattering from the sample. For a monochromatic X- ray beam of wavelength ∂, the photoelectric adsorption is expressed as:

$$I(\partial) = Io(\partial) \exp(-\rho\Delta z\mu(\partial)) \tag{3-1}$$

where, $Io(\partial)$ is the intensity of source beam and, $I(\partial)$ is the intensity of transmitted beam from a sample in the vial. ρ is the density of sample mixture and, Δz, is the diameter of the vial, which,

is fixed in the present case $\mu(\partial)$ is the mass absorption coefficient which is a function of X-ray wavelength and elemental composition of sample mixture and is studied elsewhere.[10]

For a mixture of n components, the mass absorption coefficient $\mu(\partial)$ is calculated by

$$\mu(\partial) = \sum_{i=1}^{n} \mu_i(\partial) w_i \qquad (3\text{-}2)$$

where $\mu_i(\partial)$ and w_i, are the mass absorption coefficient and the weight fraction of the ith component respectively. For the polychromatic X-ray beam of combined wavelengths range, the normalized intensity for a mixture sample is given by:

$$\frac{I}{I_o} = \sum_j a_j \exp\{-\rho \Delta z \sum_i w_i \mu_{i,j}\} \qquad (3\text{-}3)$$

where, a_j is the fraction of incident beam energy associated with j^{th} wavelength. The intensity of incident beam is controlled by the voltage, called excitation voltage and the tube current along the tungsten X-ray tube. The view cell X-ray can be operated at an excitation voltage from 30 kV to 70 kV and tube current ranges from 0.5 mA to 9.95 mA. Excitation voltage and tube current can be adjusted to obtain a good resolution and contrast for different type of samples. In this work, the excitation voltage and the tube current were 45 kV and 3.35 mA respectively.

3.4.2 Identification of coexisting phases and their volume ratios

The X- ray beam from a tungsten point source was focussed on the glass vial containing the sample mixture and the images were recorded by an x-ray sensitive image intensifier. The

images produced are 8-bit gray scale binary images of 998 by 668 pixels. At any pixel, the image intensity ranges from the maximum value 255 (white) and the minimum value zero (black). In principle, mass fractions of species in binary mixtures can be discriminated within 0.003. In this work phase volume fraction is targeted. Example images with the stirrer (right) and without the stirrer (left) are shown in Figure 3.6. In some cases, the L1/L2 phase boundary is not visible due to the limitations of the human eye, thus, the quality of such images is enhanced using histogram equalization technique[11]. Images were normalized and pixels were saturated by 0.4%. A comparison between an original and an enhanced image is shown in Figure 3.7.

The magnetic stirrer imposes an offset of 12 pixels to the L1/L2 phase boundary. The upper phase to lower phase volume ratio is determined from equation (3-4).

$$\frac{L1}{L1+L2} \; ratio = \frac{pixel\ length\ from\ the\ \frac{L1}{L2}\ boundary\ to\ the\ top\ L1\ boundary}{pixel\ length\ from\ the\ top\ L1\ to\ the\ bottom\ L2\ boundary- stirrer\ offset} \tag{3-4}$$

L1 phase = 0.715
L2 phase = 0.285

Stirrer offset = 12 ± 2 pixels
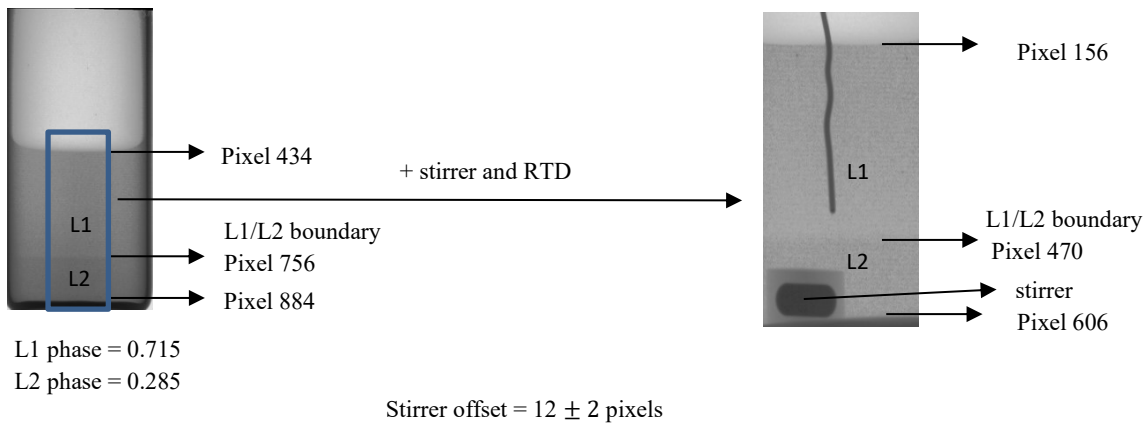
Figure 3.6. Example of an X-ray image analysis to calculate the volume ratios of L1/L2 phases
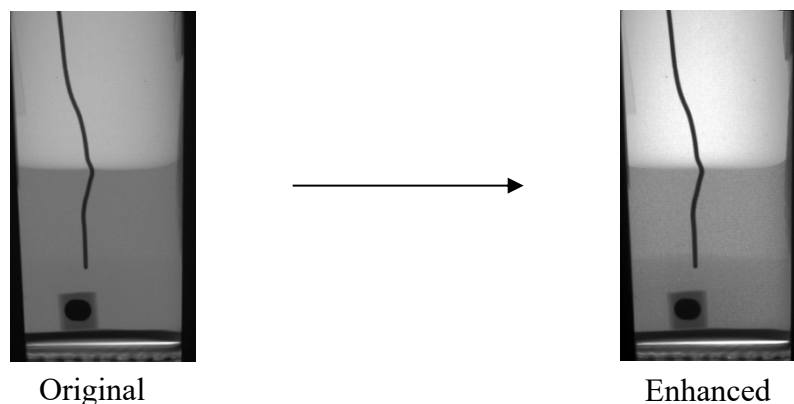
Original   Enhanced

Figure 3.7. A comparison between an original and an enhanced contrast X-ray image.

3.5 Sample Preparation Procedure

Atactic Polystyrene beads were weighed then mixed with cyclohexane in a 22 mL glass vial using a Branson 1800 Ultra-Sonicator. The polystyrene beads were miscible with cyclohexane after 5-6 hours of sonication at less than 0.05 mass fraction. At higher mass fractions, mixtures were sonicated overnight at room temperature, and two liquid phases were present. These binary mixtures were used for LL/L phase boundary measurement and UCST identification. Before a third component was added, these mixtures were heated above the upper critical solution temperature (UCST), and then the ternary mixture was placed in a vortex mixer for 90 mins. Cloud point measurements were made with ternary mixtures of polystyrene + cyclohexane + heptane or toluene, while the number of coexisting phases and phase volumes for mixtures of polystyrene + cyclohexane + nano silica mixtures were obtained using the view cell setting.

3.6   Validation of Cloud Point Measurements

The cloud point measurements were validated using literature data[12] available for mixtures of polystyrene (MW 250 kg/mol) in cyclohexane. These data were compared to experimental results for cyclohexane + polystyrene (MW 237 kg/mol) obtained in this work. Given the difference in polystyrene molar mass, the literature data should be similar but the cloud point temperatures should be systematically skewed to higher values. The UCEP should arise at a lower polymer mass fraction and at a higher temperature than in this work.[13] The expected trend and skew are evident in Figure 3.8. The reported uncertainty for the data of Shultz and Flory[12] is 0.4 K in temperature and $\pm$ 0.005 uncertainty in the volume fraction of polystyrene. This work has an uncertainty of 0.3 K in temperature and $\pm$ 0.005 uncertainty of volume fraction of polystyrene.
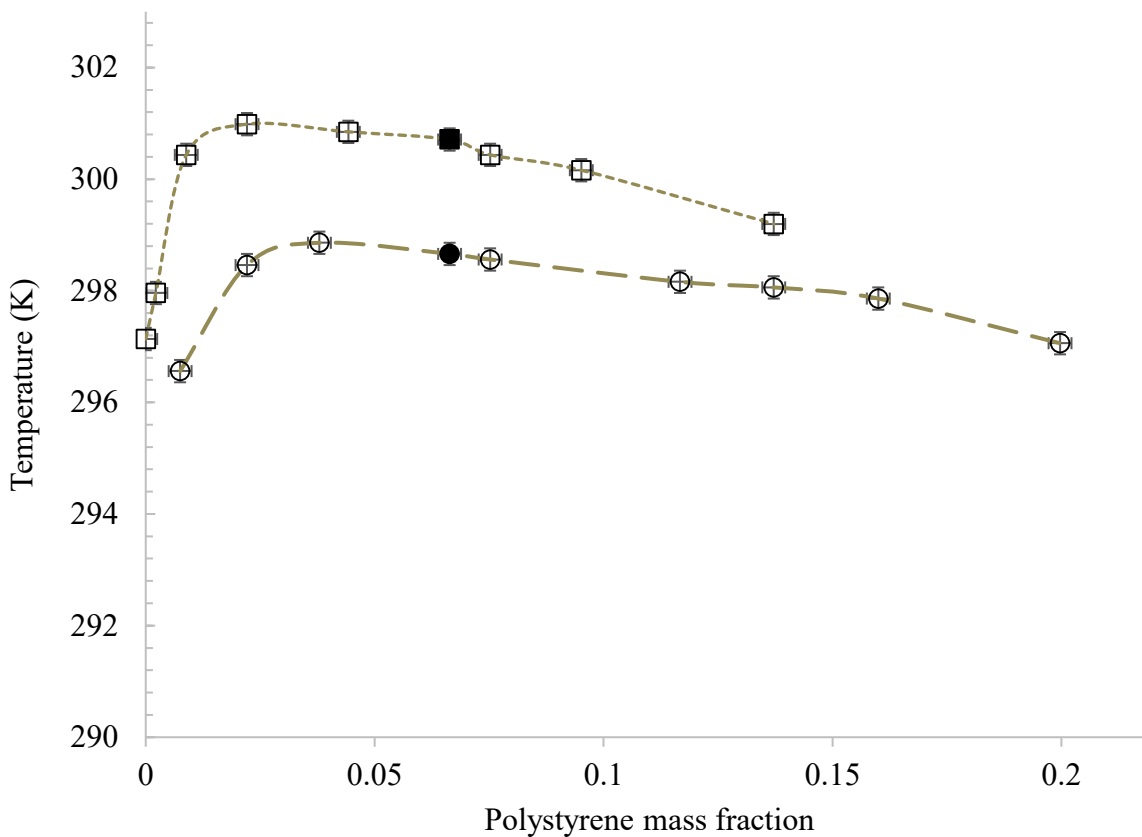
Figure 3.8. Cloud point data for binary polystyrene + cyclohexane mixture. Symbols: (⬤) this work for polystyrene MW 237 kg/mol and (◻) literature[12] for polystyrene MW 250 kg/mol. Filled markers represent critical points.

3.7   Validation of Phase Volume Measurements

The number of coexisting phases and respective phase volumes were obtained using the X-ray view cell setup. A volume calibration curve was prepared for the standard 22 mL-glass vial using deionized water. The pixel elevation as a function of volume in the vial is shown in Figure 3.9.
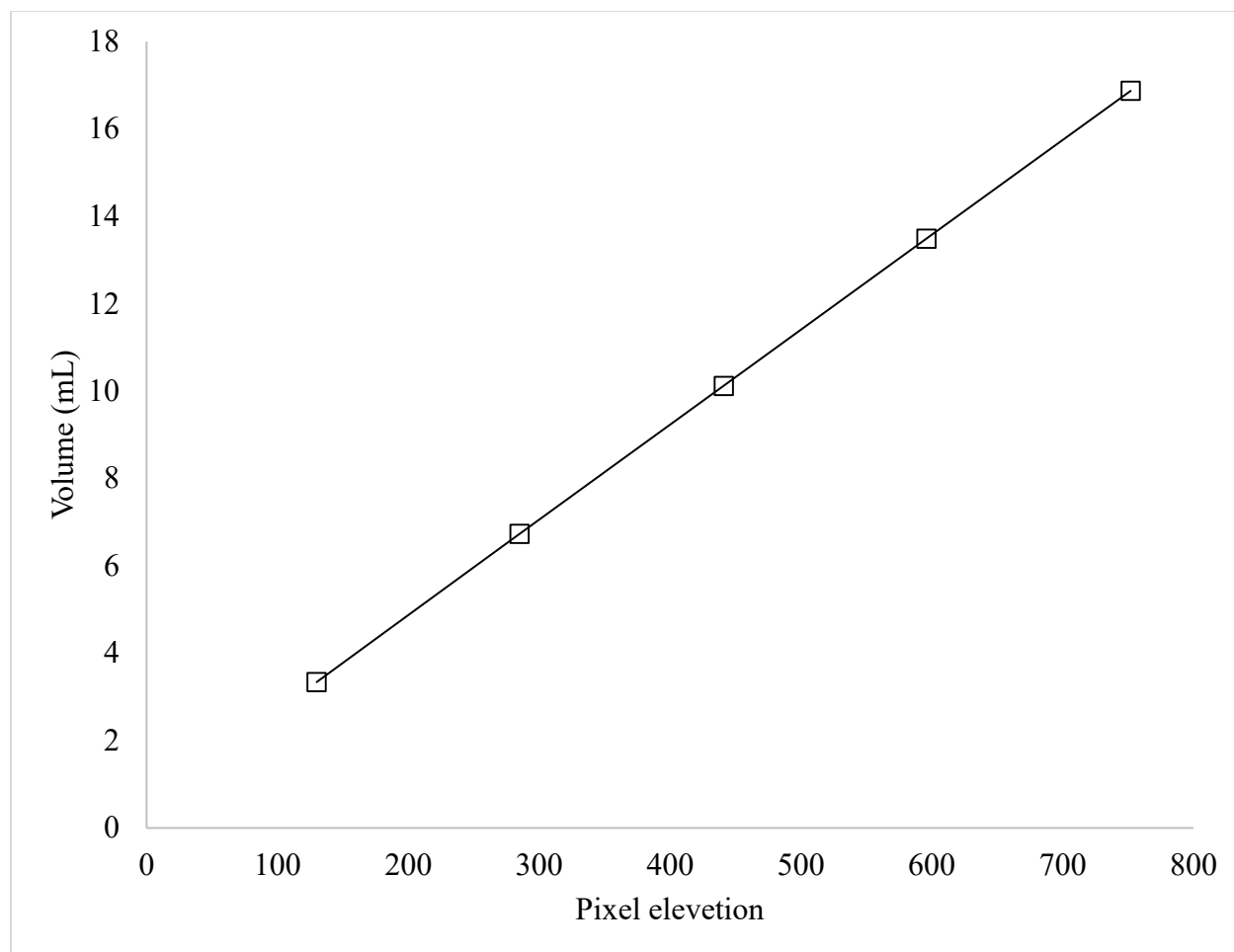
Figure 3.9. Liquid volume as a function of pixel number for standard 22 mL glass vials. Symbol: (⧈) experimental data point.

Further to ensure that the modified view cell setup provides accurate relative phase volumes, a 7:3 (by mass) mixture of glycerol: 1-pentanol was prepared in a glass vial and heated above upper critical solution temperature and then cooled down to 296 K. This mixture shows two-phase behaviour at 296 K.[14] Another 7:3 mixture was prepared in a graduated cylinder. Since, visualization of the two phases was feasible with the naked eyes, the reading from the graduated cylinder (uncertainty $\pm$ 0.02) was compared against the reading of the mixture prepared in the glass vial. The same validation pattern has been used for different volumes of same mixture and

data has been reported in Table 3.3. The absolute average deviation was found to be 0.02 (Table 3.2). The uncertainty includes following assumptions:

(a) constant diameter glass vials, and

(b) small deviations in predicting L1/L2 phase boundary ($\pm$ 2 pixel)

Table 3.2. X-ray view cell validation

Sample No.	L1/(L1+L2) volume ratio using equation (3-4), and X ray image analysis	L1/(L1+L2) volume ratio using graduated cylinder (uncertainty $\pm$ 0.02)	Difference between L1/(L1+L2) volume ratios calculated using a graduated cylinder and X-ray analysis
1	0.52	0.51	0.01
2	0.49	0.51	-0.02
3	0.47	0.47	0.00
4	0.51	0.52	-0.01
5	0.50	0.50	0.00
6	0.49	0.49	0.00

3.8 Phase Boundary Validation

A validation experiment with polystyrene (MW 237 kg/mol) + cyclohexane mixture was done at 296 K to calculate phase boundary compositions and compared against the last validation result (Figure 3.8). The polystyrene rich phase was recorded using view cell setup and shown in Figure 3.10. A straight line can be drawn through the experimental data points and can extrapolated further to find the two-liquid to single liquid phase transition compositions for polystyrene + cyclohexane mixture at 296 K. Table 3.3 shows the extrapolated and experimental liquid-liquid to liquid transition (cloud point) compositions of polystyrene + cyclohexane mixture at 296 K. The average deviation observed is 0.02.
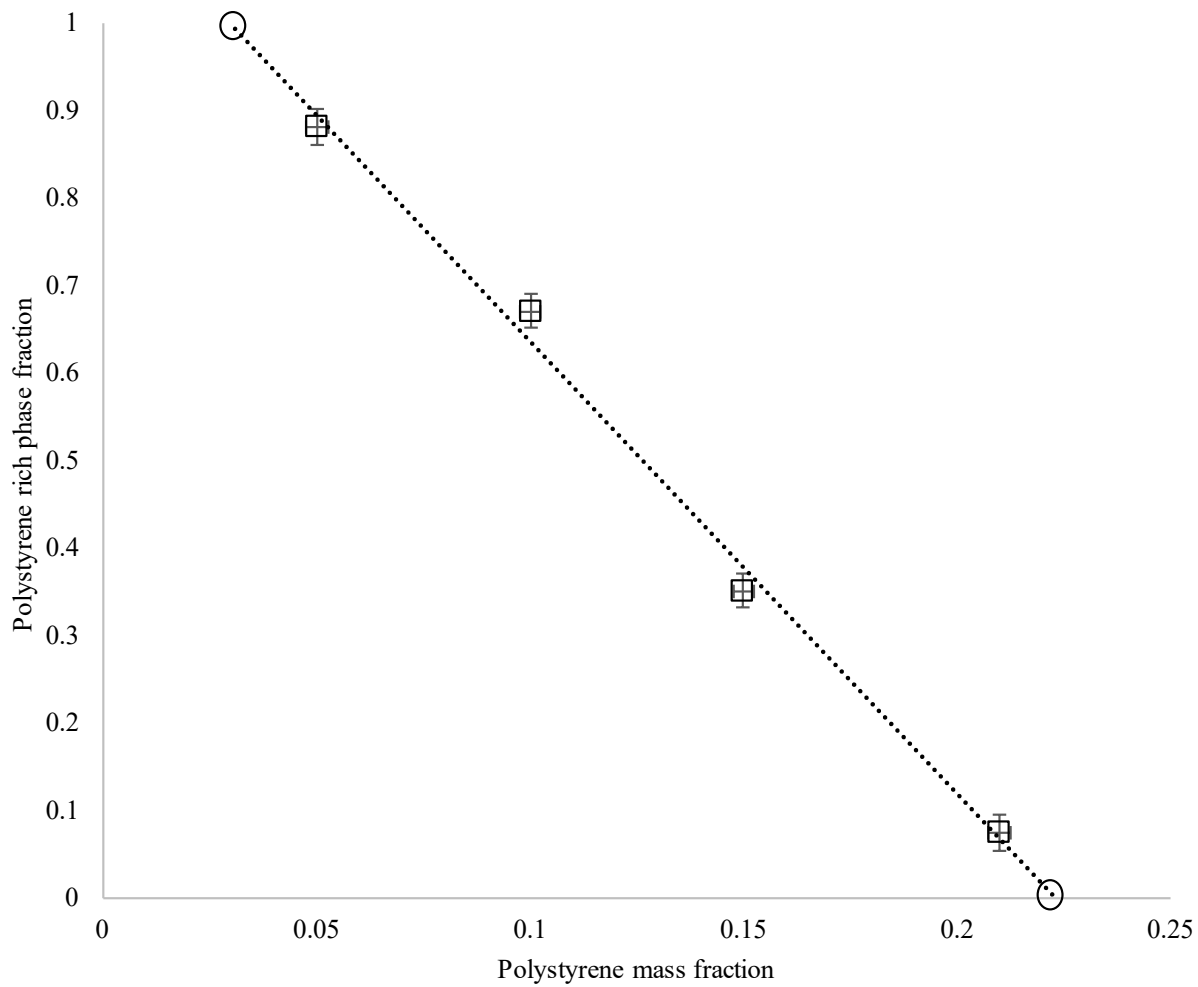
Figure 3.10. Polystyrene rich phase fraction variation as a function of polystyrene mass fraction in cyclohexane. Symbol: (▢) experimental data using X-ray view cell and (⊙) extrapolated cloud points.

Table 3.3. Phase boundary composition in polystyrene + cyclohexane mixture at 296 K

Polystyrene mass fraction (X-ray view cell)	Polystyrene rich phase fraction	Polystyrene mass fraction (Extrapolated cloud point composition)	Phase boundary composition (Figure 3.8) $\pm$ 0.01
	1.00	0.02	0.01
0.05	0.88	--	--
0.10	0.67	--	--
0.15	0.35	--	--
0.21	0.07	--	--
	0.00	0.21	0.20

3.9   Nomenclature

HPLC   high pressure liquid chromatography

RI   refractive index

C_7 n-heptane

RTD   resistance temperature detector

I_o source intensity

I transmitted intensity

∂ wavelength

ρ density of sample mixture

Δz diameter of the vial

μ mass absorption coefficient

w_i weight fraction of the ith component

a_j fraction of incident beam energy associated with j^{th} wavelength

L1   low density liquid

L2   high density liquid

UCST   upper critical solution temperature

3.10 References

1.   Wünsch, Josef Richard. Polystyrene: Synthesis, production and applications. Vol. 112. iSmithers Rapra Publishing, **2000**.

2.   Koningsveld, R.; Kleintjens, L. A.; Shultz, A. R. Liquid–liquid phase separation in multicomponent polymer solutions. IX. Concentration-dependent pair interaction parameter from critical miscibility data on the system polystyrene–cyclohexane. Journal of Polymer Science Part A-2: Polymer Physics **1970**, 8, 1261-1278.

3.   Koningsveld, R.; Kleintjens, L. A. Liquid-liquid phase separation in multicomponent polymer systems. X. Concentration dependence of the pair-interaction parameter in the system cyclohexane-polystyrene. Macromolecules **1971**, 4, 637-641.

4.   Kuwahara, N.; Nakata, M.; Kaneko, M. Cloud-point curves of the polystyrene-cyclohexane system near the critical point. Polymer **1973**, 14, 415-419.

5.   Abedi, S. J.; Cai, H. -Y.; Seyfaie, S.; Shaw, J. M. Simultaneous phase behaviour, elemental composition and density measurement using X-ray imaging. Fluid Phase Equilibria **1999**, 158, 775-781.

6.   Zou, X. Selective removal of inorganic fine solids, heavy metals and sulfur from bitumen/heavy oils; University of Toronto: **2003**.

7.   Zou, X.; Zhang, X.; Shaw, J. Phase Behavior of Athabasca Vacuum Bottoms + n-Alkane Mixtures. SPE Production & Operations **2007**, 22, 265-272.

8.   Amani, M. J.; Gray, M. R.; Shaw, J. M. On correlating water solubility in ill-defined hydrocarbons. Fuel **2014**, 134, 644-658.

9.   Dini, Y.; Becerra, M.; Shaw, J. M. Phase Behavior and Thermophysical Properties of Peace River Bitumen Propane Mixtures from 303 K to 393 K. Journal of Chemical & Engineering Data **2016**, 61, 2659-2668.

10.   De Boer, D. Fundamental parameters for X-ray fluorescence analysis. Spectrochimica Acta Part B: Atomic Spectroscopy **1989**, 44, 1171-1190.

11.   Pizer, S. M.; Amburn, E. P.; Austin, J. D.; Cromartie, R.; Geselowitz, A.; Greer, T.; ter Haar Romeny, B.; Zimmerman, J. B.; Zuiderveld, K. Adaptive histogram equalization and its variations. Computer vision, graphics, and image processing **1987**, 39, 355-368.

12.   Shultz, A. R.; Flory, P. J. Phase Equilibria in Polymer—Solvent Systems1, 2. J. Am. Chem. Soc. **1952**, 74, 4760-4767.

13.   Kamide, K.; Matsuda, S.; Dobashi, T.; Kaneko, M. Cloud point curve and critical point of multicomponent polymer/single solvent system. Polym. J. **1984**, 16, 839-855.

14.   Matsuda, H.; Fujita, M.; Ochi, K. Measurement and correlation of mutual solubilities for high-viscosity binary systems: aniline methylcyclohexane, phenol heptane, phenol octane, and glycerol 1-pentanol. J. Chem. Eng. Data **2003**, 48, 1076-1080.

Chapter 4. Results and Discussion

4.1   Background and Validation Measurements

Calibration and methods validation measurements are reported in Chapter 3. Cloud point temperatures, global and individual phase compositions, and phase volumes ratios have a repeatability within 0.3 K, 0.005 and 0.03 respectively.   For example, cloud points for polystyrene (MW 237 kg/mol) + cyclohexane were obtained experimentally using the cloud point setup displayed in Figure 3.2 and validated against the best available literature data as shown in Figure 3.8. The sensitivity of cloud point temperatures for cyclohexane + polystyrene binary mixtures to trace amounts of toluene and heptane (C_7) was also evaluated as part of the background measurements to demonstrate the impact of a compound miscible with polystyrene and cyclohexane (toluene) and immiscible with polystyrene (heptane) on the observed phase behaviour. As expected, the addition of toluene reduced the cloud point temperature while the addition of heptane (C_7), raised the cloud point temperature. The results are shown in Figure 4.1. The impact is secondary. At 0.083 C_7 mass fraction in a polystyrene + cyclohexane mixture the cloud point temperature goes up $\sim$ 10 K. For toluene addition, the cloud point temperature decreases $\sim$ 10 K at 0.05 toluene mass fraction.
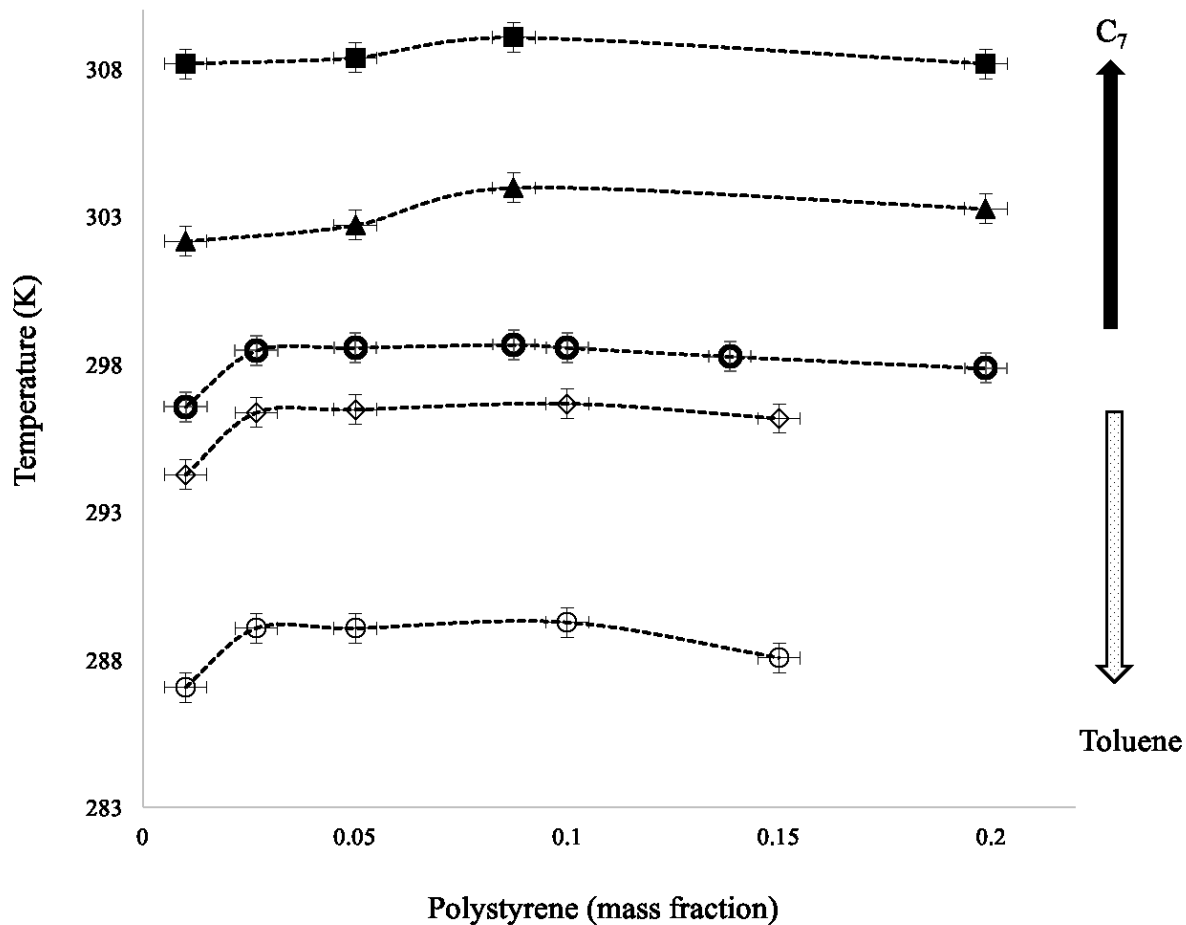
Figure 4.1. Effect on the cloud points of polystyrene + cyclohexane mixture with the addition of toluene and heptane (C_7). Symbols: (⬤) cyclohexane only, (◇) 0.01 mass fraction toluene, (○) 0.05 mass fraction toluene, (▲) 0.045 mass fraction C_7, and (■) 0.083 mass fraction C_7.

4.2   Illustrative Measurements for Fumed Silica Nanoparticles (7 nm) + Polystyrene (MW 237 kg/mol) + Cyclohexane Mixtures

Preliminary and illustrative experiments were performed at 295 K using 22 mL glass vials and visible light. The results are shown in Figure 4.2. Cyclohexane, Figure 4.2 (a), is a clear single-phase liquid. Cyclohexane + silica nanoparticle binary mixtures form a single-phase colloid as shown in Figure 4.2 (b). Silica nanoparticles remain dispersed in cyclohexane and settling is not observed up to ~ 48 hrs. Polystyrene (0.1 mass fraction) + cyclohexane exhibits liquid-liquid phase behavior. The polystyrene rich phase is the lower phase, and cyclohexane rich phase is the upper phase - Figure 4.2 (c). For silica nanoparticles (0.01 mass fraction) + a (polystyrene (0.1 mass fraction) + cyclohexane mixture, the relative phase volumes of the two liquids changes dramatically - Figure 4.2 (d). The silica particle rich phase is the lower phase and the polystyrene rich phase is the upper phase.

Figure 4.2. Vials (a) cyclohexane, (b) cyclohexane + silica nanoparticles (0.01 mass fraction), (c) cyclohexane + polystyrene (0.10 mass fraction), and (d) cyclohexane + polystyrene (0.10 mass fraction) + silica nanoparticles (0.01 mass fraction) at 295 K.

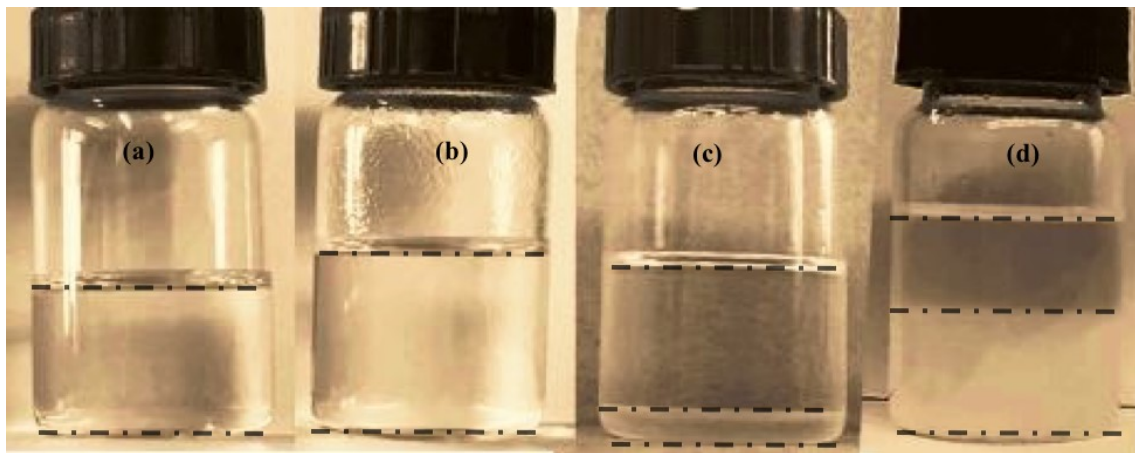The transition of a colloid gas (G) phase to coexisting colloid gas + liquid (G+L) phases and to a colloid liquid (L) phase is observed when enough silica nanoparticles are added to fixed compositions of polystyrene + cyclohexane binary mixtures at 296 K (below the UCEP) and 303 K (above the UCEP). Volume fractions of G and L phases were measured and even at low silica nanoparticle mass fractions (0.0005 mass fraction), colloid gas (G) and colloid liquid (L) phases co-exist. As the silica nanoparticle mass fraction increases, the volume fraction of G decreases. An example is shown in Figure 4.3. Within the GL region the volume fractions of the two phases are also a function of temperature as illustrated in Figure 4.4, where the volume fraction of coexisting phases at 296 K and 303 K for four sets of fixed silica nanoparticle + polystyrene + cyclohexane phase equilibrium experiments are presented.

Outcomes from more extensive and detailed sets of experiments, showing upper and lower silica nanoparticles mass fraction limits for GL behavior in some cases, are reported in Figure 4.5. Figure 4.5 (a) and (b) are very dilute solutions of polystyrene in cyclohexane and GL regions are confined within small mass fractions of nano silica. For a 0.05 mass fraction of polystyrene in cyclohexane (Figure 4.5 (c)), no transition from colloid gas (G) to coexisting colloid gas and liquid G+L phase is observed except at very low concentration of polystyrene (< 0.03 mass fraction). Figure 4.5 (d), (e) and (f) show a threshold limit of silica nanoparticle concentration at 296 K up to which there were no significant change in the colloid gas (G) relative volume is observed. At 303 K, transition from colloid gas (G) to coexisting colloid gas + liquid (G+L) and finally to the colloid liquid (L) phases remain consistent. The colloid gas + liquid (G+L) → colloid liquid (L) phase boundary curve is monotonically increasing in nature as silica nanoparticle composition and composition of polystyrene in the mixture were increased. For a

0.095 mass fraction of polystyrene in cyclohexane at 296 K, the nanoparticle composition recorded for the G+L → L transition was 0.053 mass fraction and is the maxima of phase boundary curve. Above this concentration, G+L → L boundary curve starts decreasing with negative slope as the concentration of polystyrene increases in the ternary mixture. Similar trends were observed at 303 K.
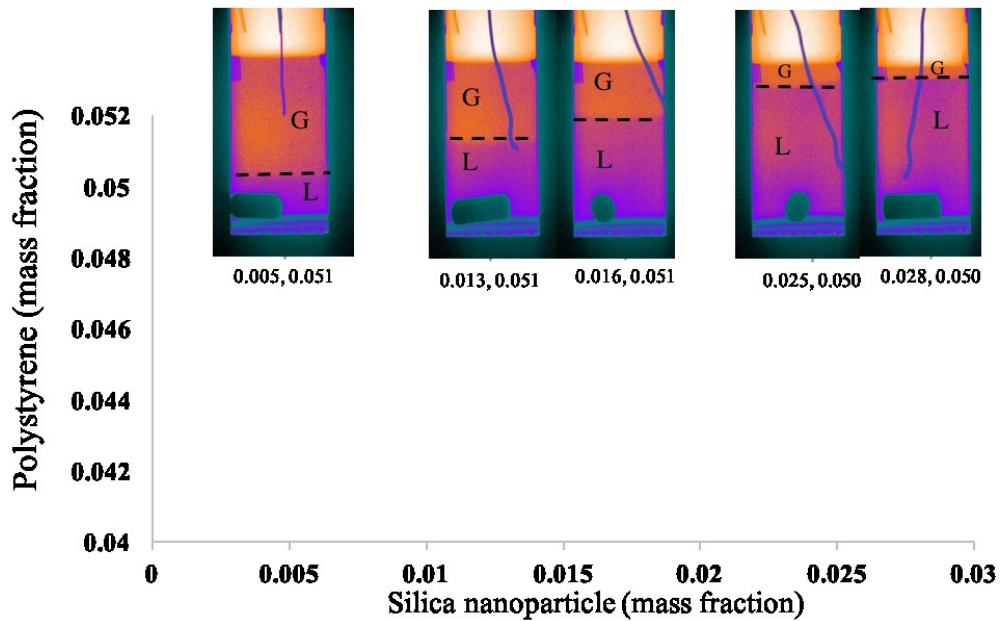
Figure 4.3. Coexisting phases relative volumes as a function of nano silica mass fraction in a (1:19) polystyrene: cyclohexane mixture at 296 K. Symbols: (G) colloid gas and (L) colloid liquid phase.
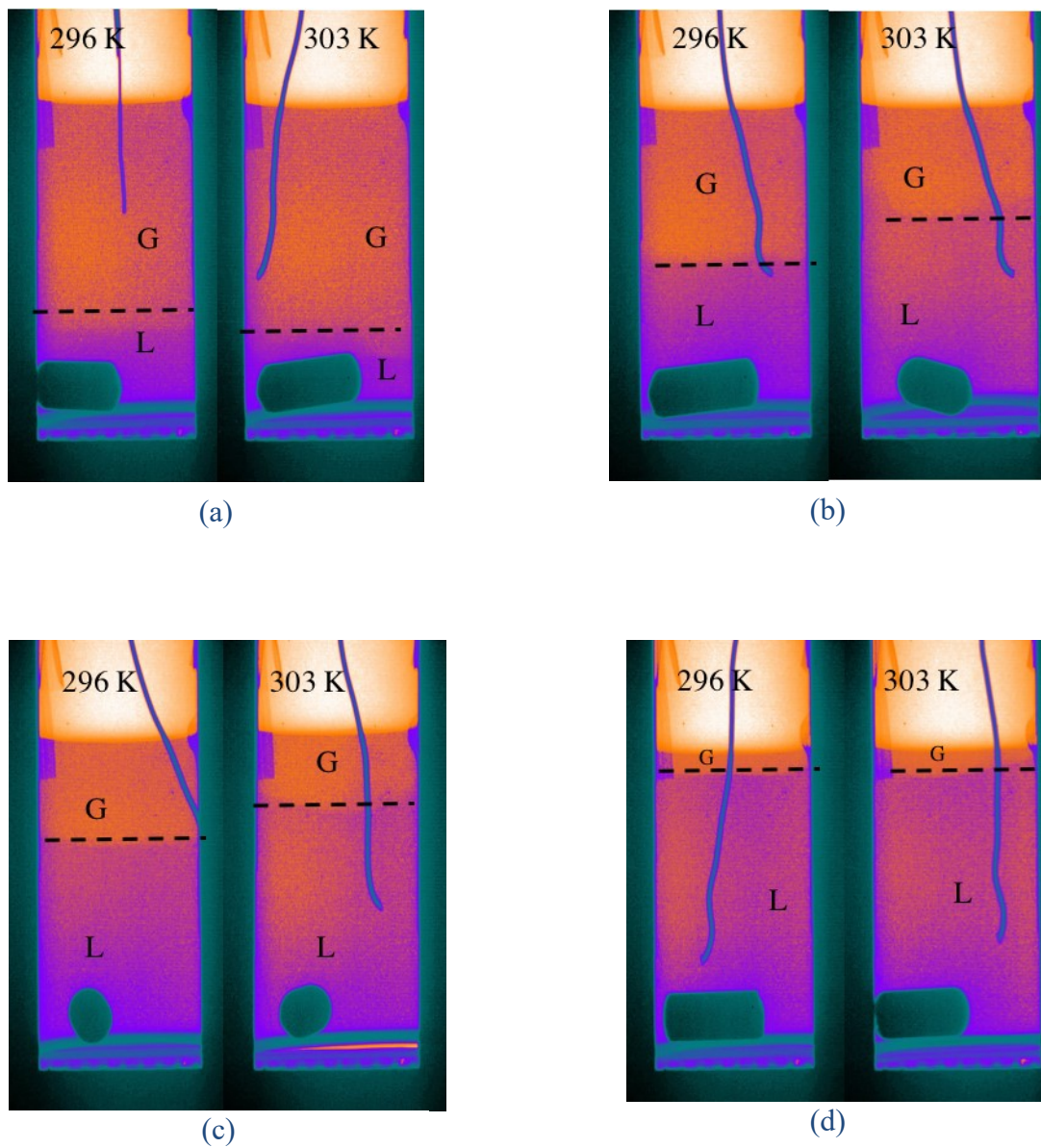
Figure 4.4. Impact of temperature at fixed composition (1:19) polystyrene: cyclohexane mixture.

Silica nanoparticle mass fraction varies (a) 0.005, (b) 0.013, (c) 0.025, (d) 0.016

(e)

(f)
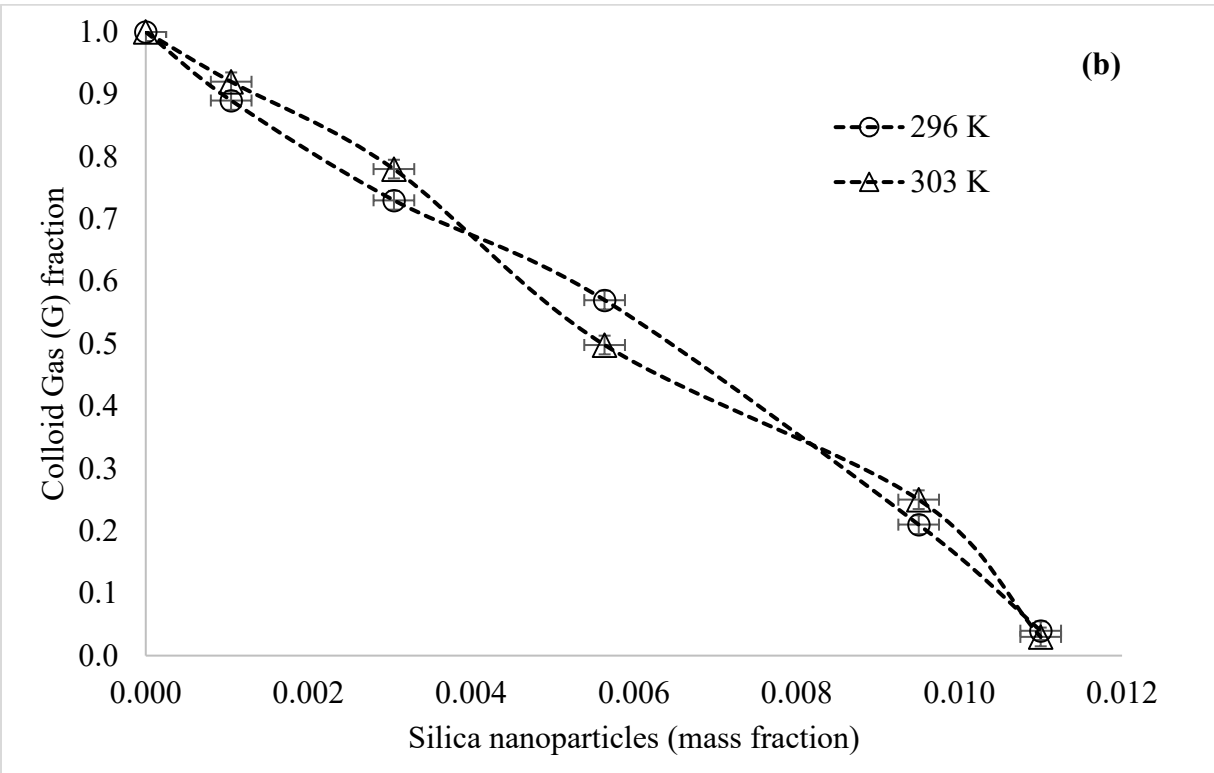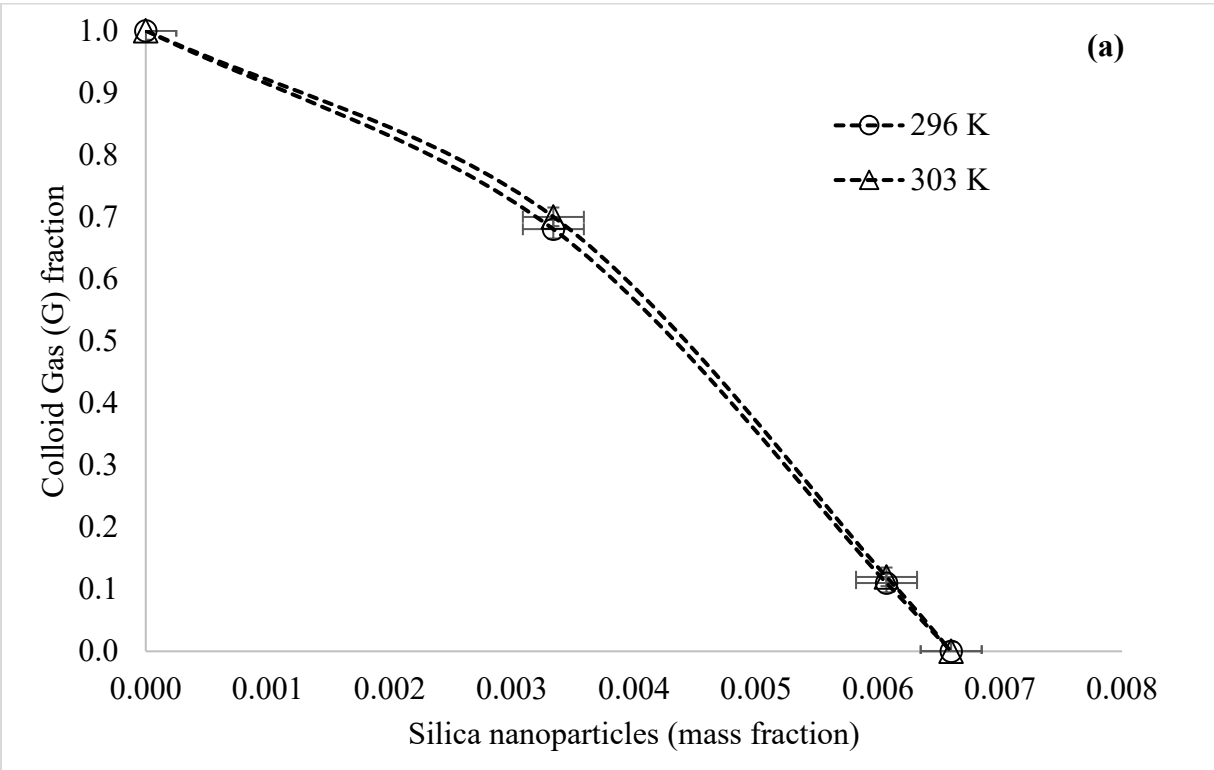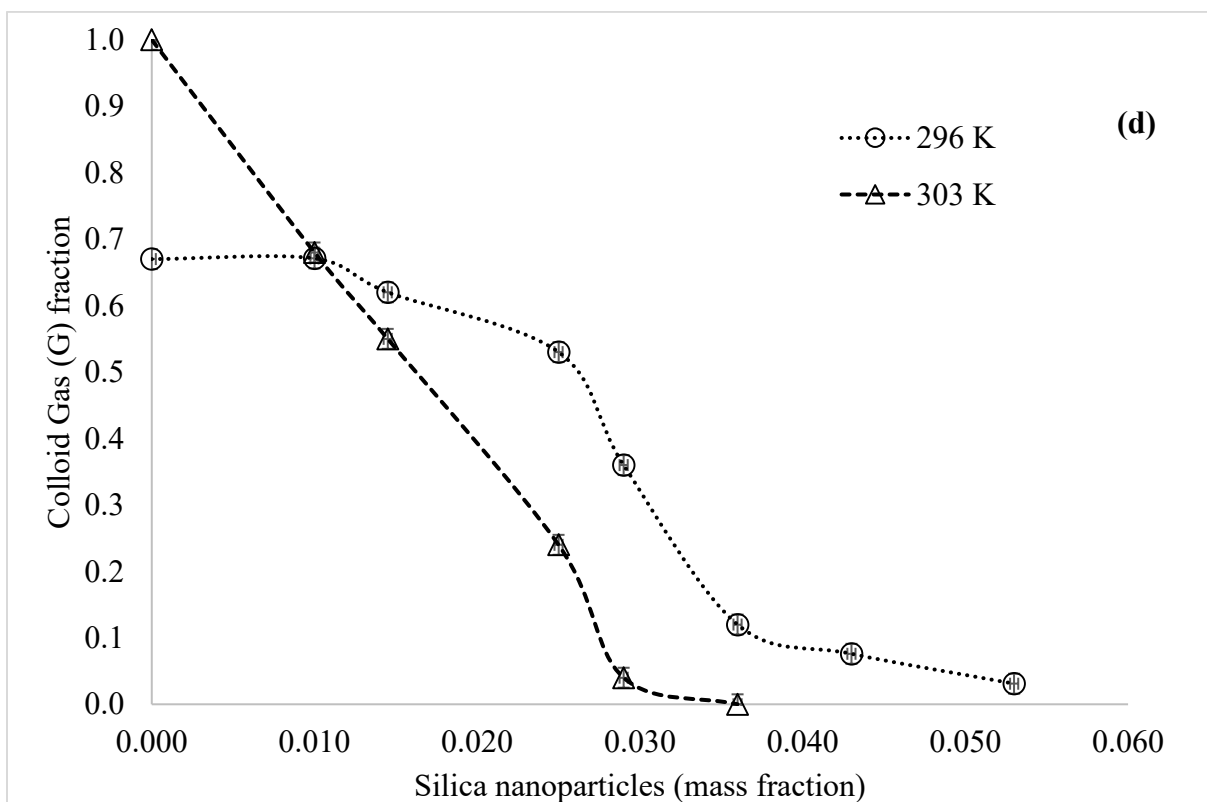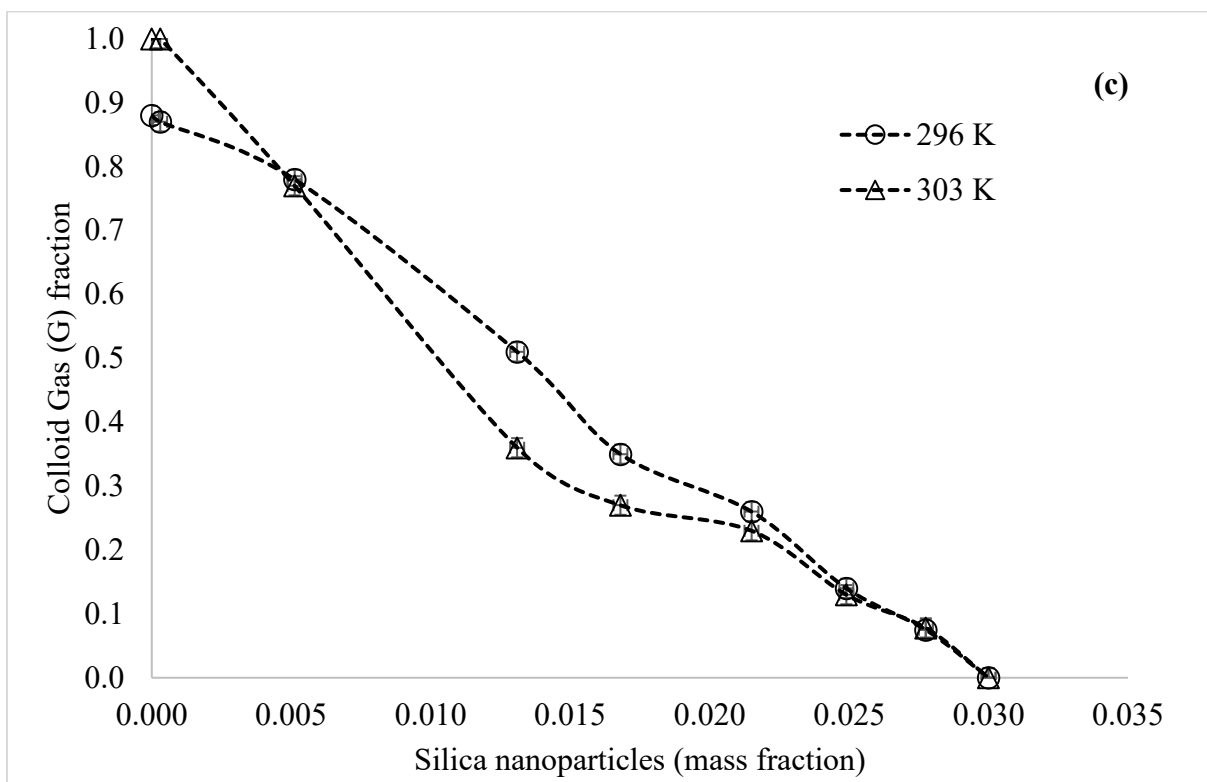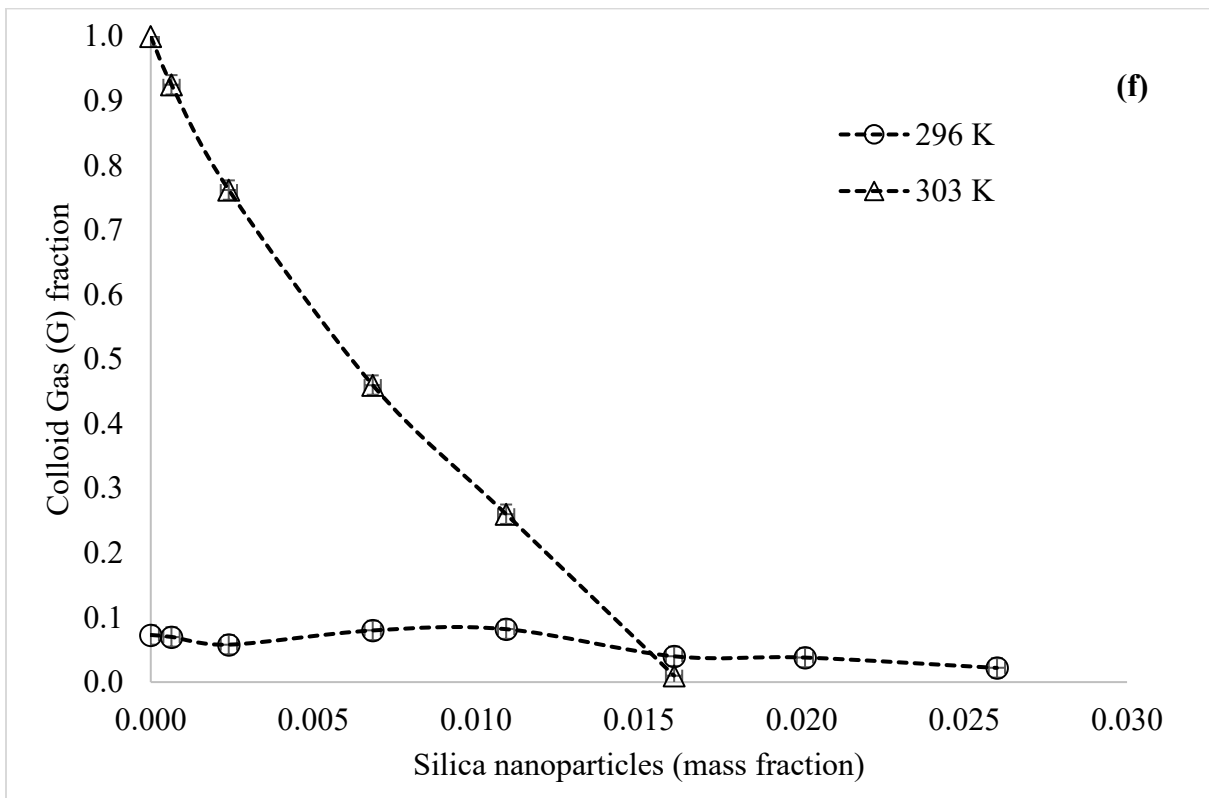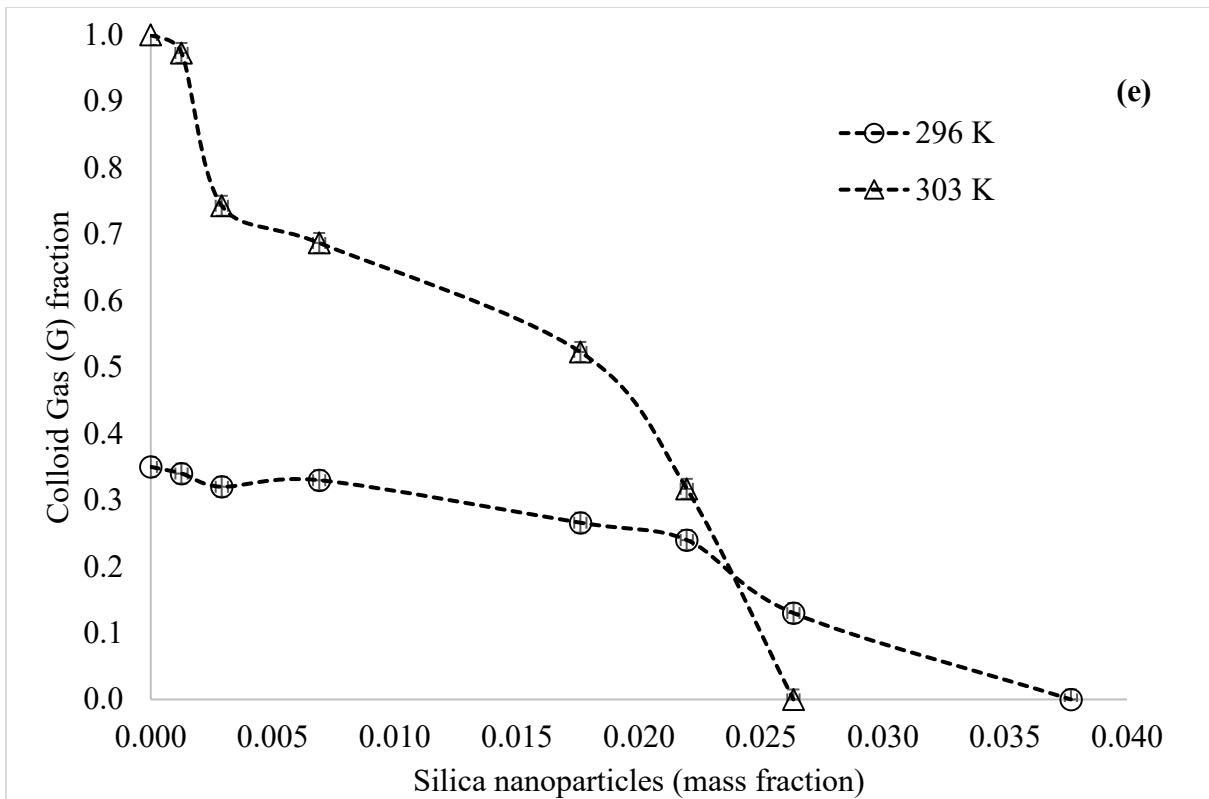
Figure 4.5. Colloid gas volume fraction as a function of silica nanoparticle mass fraction at fixed polystyrene + cyclohexane composition: (a) polystyrene (0.0039 mass fraction) + cyclohexane mixture, (b) polystyrene (0.0105 mass fraction) + cyclohexane mixture, (c) polystyrene (0.05 mass fraction) + cyclohexane mixture, (d) polystyrene (0.10 mass fraction) + cyclohexane mixture, (e) polystyrene (0.15 mass fraction) + cyclohexane mixture, and (f) polystyrene (0.21 mass fraction) + cyclohexane mixture. Symbols: (O) 303 K and (△) 296 K. Dotted curves are intended to guide the eye.

At 296 K, experimental data suggest a colloid gas like (G) phase at very low concentration of polymer and nanoparticles in cyclohexane. A G=L critical point is expected at 0.00016 mass fraction of polystyrene and 0.003 mass fraction of nanoparticles as shown in Figure 4.6 & 4.7 (close up of the phase boundary region).
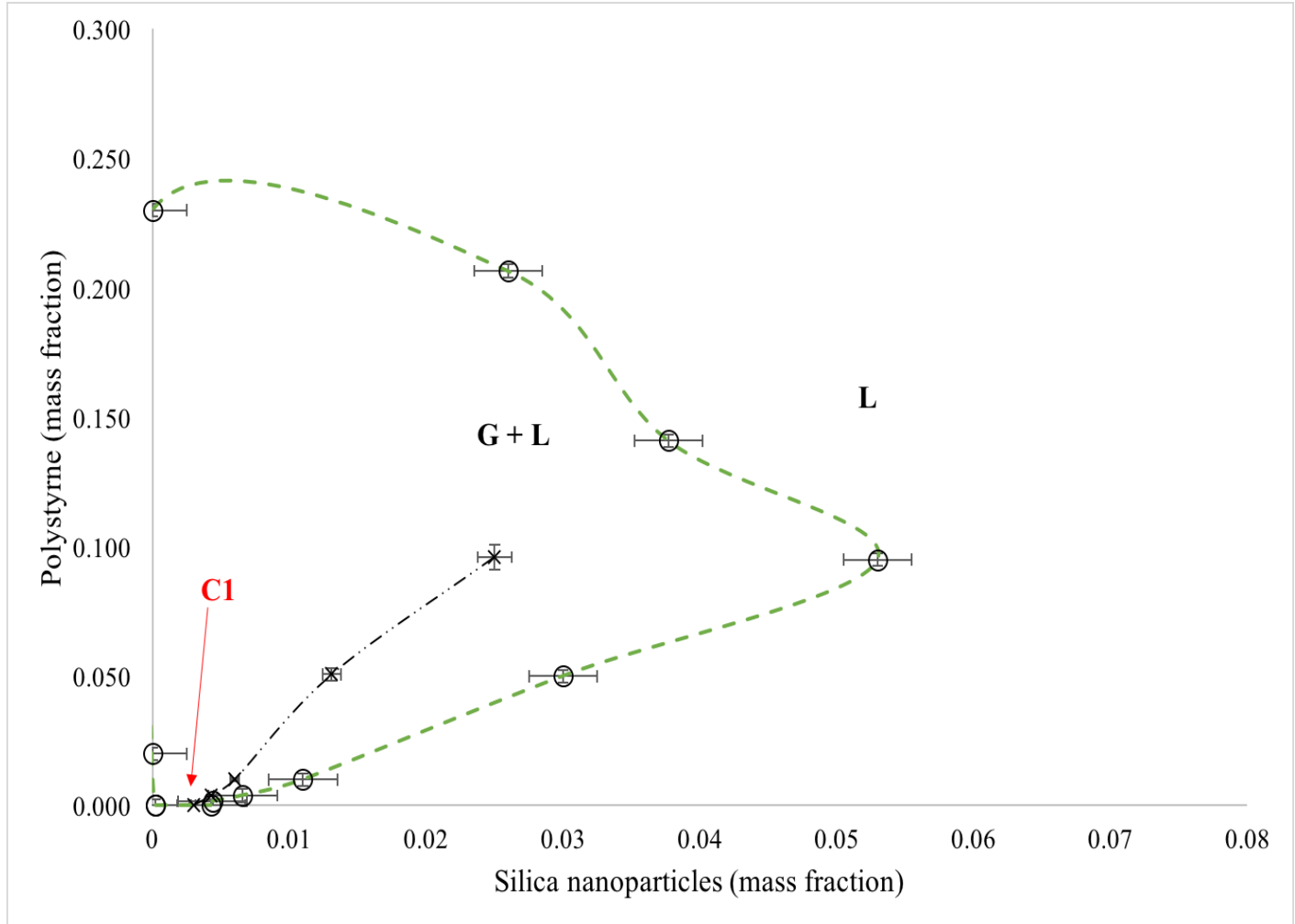
Figure 4.6. Experimental phase diagram of cyclohexane + polystyrene + silica nanoparticles at 296 K. (G) colloid gas like phase, (L) colloid liquid like phase, (G+L) coexisting colloid liquid like and gas like phases, (O) phase boundary, (x) G=L=0.5 (volume fraction) and (C1) critical point.
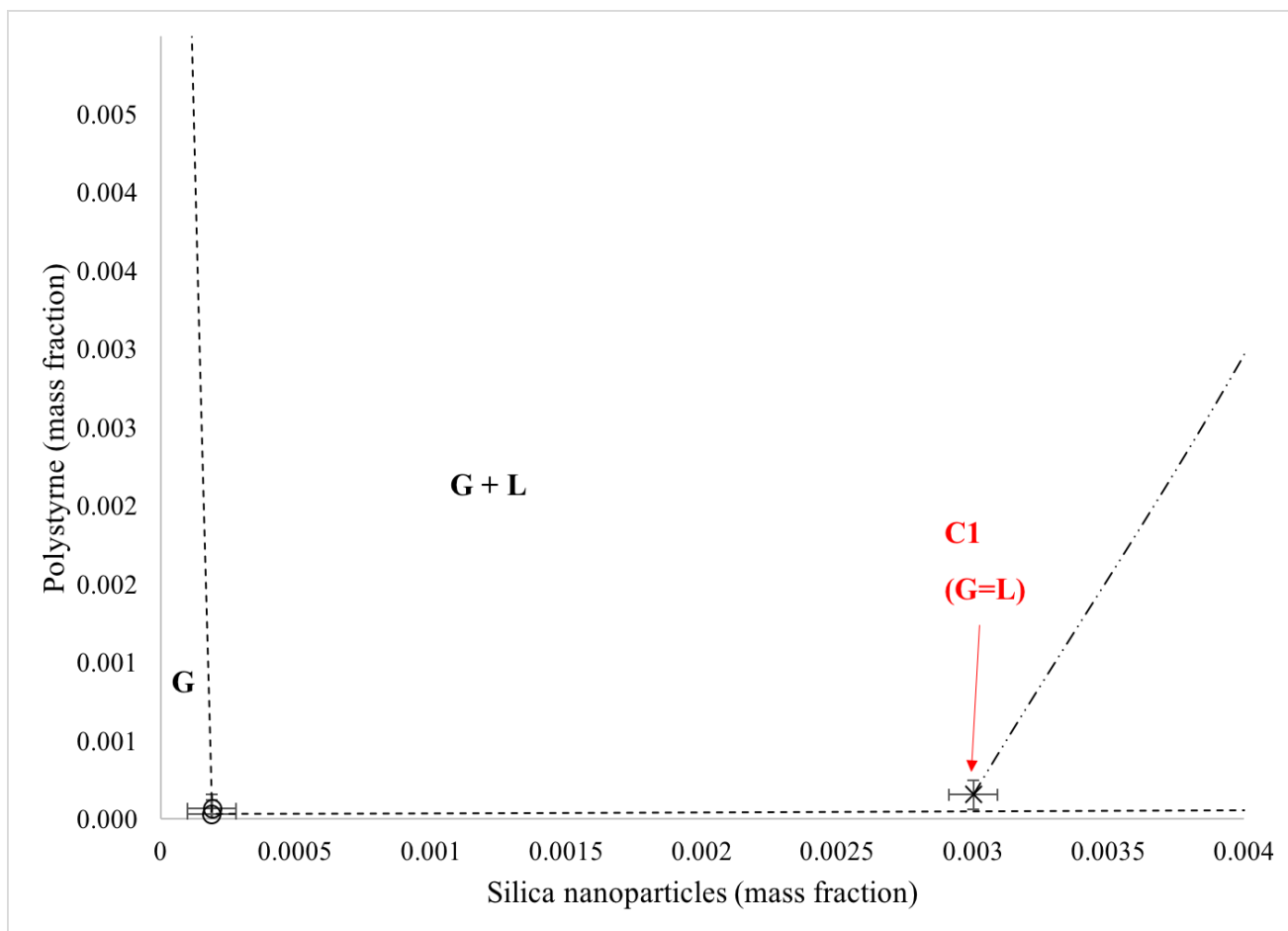
Figure 4.7. Prediction of critical point C1 of cyclohexane + polystyrene + silica nanoparticles mixture at 296 K. Figure 4.6 plotted again to demonstrate the location of the critical point, C1. Symbols: (O) phase boundary, (x) G=L=0.5 (volume fraction) and (C1) critical point at 0.003 nano silica mass fraction and 0.00016 polystyrene mass fraction (uncertainty $\pm$ 0.00005).

Vials with a nominal volume from 40 mL to 100 mL were used to report small concentrations accurately with adequate accuracy ($\pm$ 0.01). Critical points on the G + L boundary were identified by extrapolating plots of relative volume fraction of colloid gas (G) = relative volume fraction of colloid liquid (L) = 0.5 to the G+L phase boundary.

At 303 K, GL region is bounded by colloid gas (G) and liquid (L) phases (Figure 4.8). The critical point C1 has the same composition as at 296 K (Figure 4.6). The critical point C2 (0.275 mass fraction of polystyrene and 0.006 mass fraction of silica nanoparticles) has a higher polymer concentration. The phase boundary peak was observed at 0.036 mass fraction of silica nanoparticles and 0.096 mass fraction of polystyrene. The G+L to G and the G + L to L phase boundaries at 296 K and 303 K are compared in Figure 4.9. There are both qualitative and quantitative differences in the phase behaviors at these two temperatures. At 303 K, the G + L region comprises a closed loop in the phase diagram while at 296 K, the G + L region begins at the zero nanoparticle mass fraction axis. From a quantitative perspective, the G + L region shrinks in size as the temperature increases.
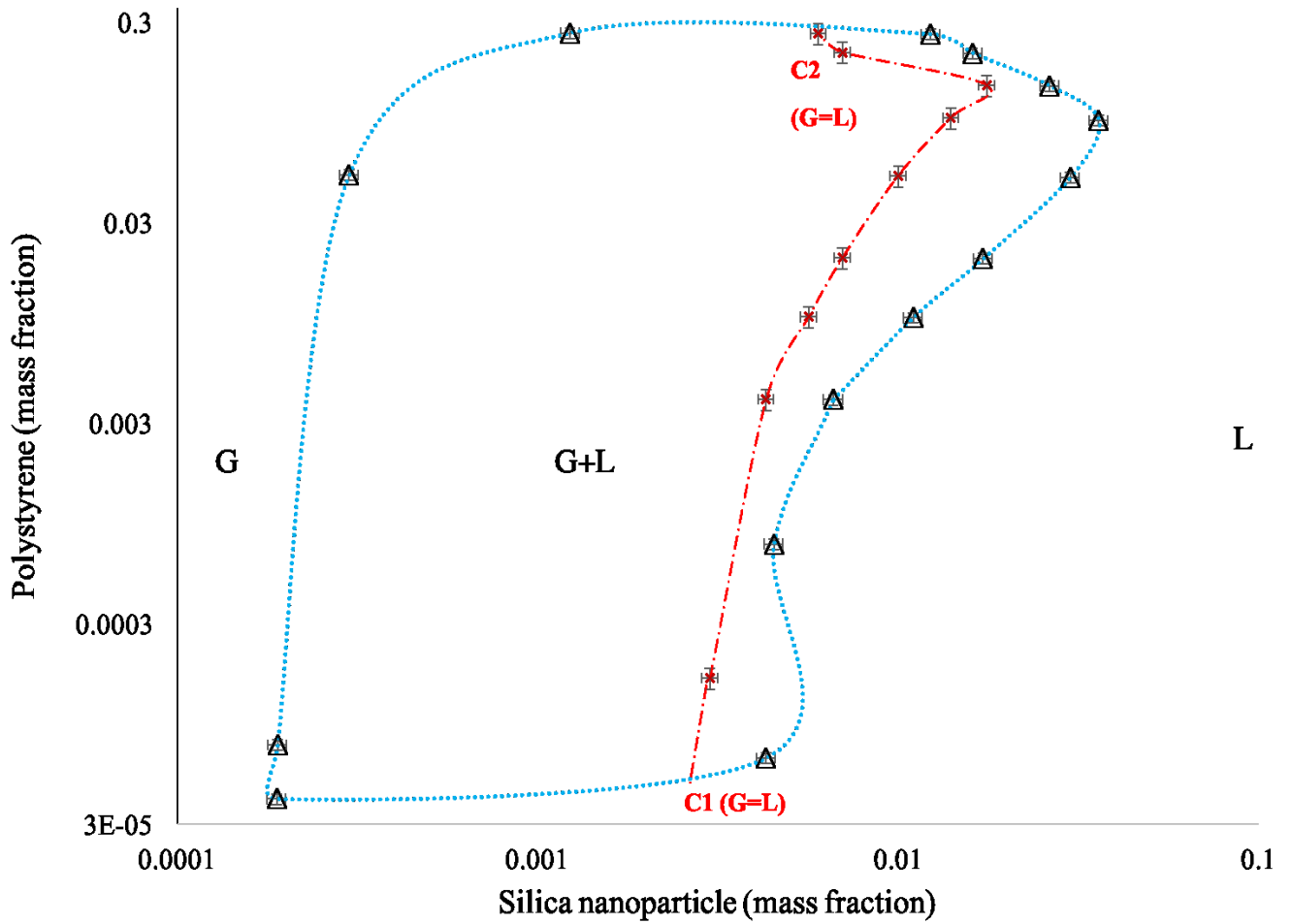
Figure 4.8. Experimental phase diagram of cyclohexane + polystyrene + silica nanoparticles at 303 K. (△) G+L phase boundary, and (x) G=L=0.5 (volume fraction), (C1) first critical point, and (C2) second critical point.
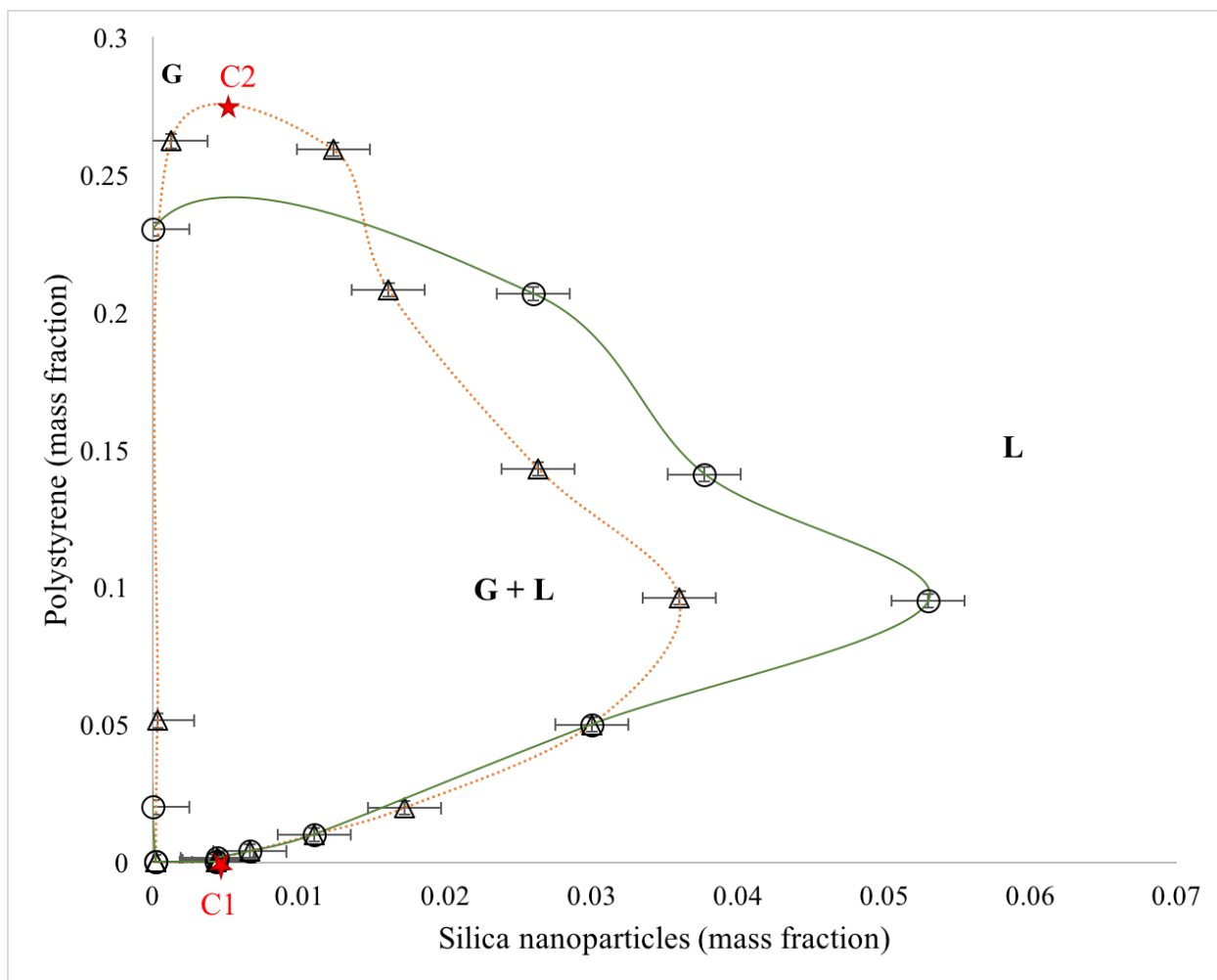
Figure 4.9. Experimental phase diagram of cyclohexane + polystyrene + silica nanoparticles mixture. (○) G+L phase boundary at 296 K, (△) G+L phase boundary at 303 K, (★, C1) first critical point, and (★, C2) second critical point.

4.3   Sensitivity of the Polystyrene + Cyclohexane Binary Liquid-Liquid to Liquid

Phase Boundary with Solvent Composition

Polystyrene + cyclohexane binary mixtures show a liquid-liquid to liquid phase boundary and an upper critical end (UCEP) point.[1-4] In this work, polystyrene MW 237 kg/mol in cyclohexane exhibits an UCEP at 299 K and one liquid phase is marginally stable just above UCEP and two liquid-like phases coexist at a temperature below the UCEP. The liquid-liquid phase behavior in this mixture is attributed to the transformation of the polymer from a coil form to a globule form. The radius of gyration of polystyrene coils in cyclohexane decreases from ~13 nm above the UCEP temperature to ~ 5 nm below the UCEP temperature.[5-7] The entropic interaction between polymer coils and solvent molecules is favorable above UCEP and a single liquid phase is stable. Below the UCEP temperature, polymer-polymer entropically driven interaction is favorable. Phase separation into a polymer rich and solvent rich phases arises from molecular interactions. The liquid-liquid to liquid phase boundary for polystyrene + cyclohexane mixtures is sensitive to small changes in solvent composition. Toluene shifts this boundary to lower temperatures because polystyrene and cyclohexane are both miscible in toluene. Heptane shifts this boundary to higher temperatures because polystyrene is not miscible in heptane irrespective of its conformation.

4.4 Effect of Silica Nanoparticles on the Phase Behavior of Polystyrene + Cyclohexane Binary Mixtures

The addition of nanoparticles (on which polymer does not adsorb) to miscible polymer + solvent mixtures leads to phase separation, at any temperature, that is driven by the depletion flocculation mechanism.[8] This effect is observed when the radius of gyration of polymer coils (R_g) is comparable to the nanoparticles size (a). The cases for which $a \gg R_g$ and $a \ll R_g$, result in a regular colloid phase diagram exhibiting equilibrium between colloid fluid like and colloid nanoparticle rich phases. The radius of gyration, R_g, of polystyrene (MW 237 kg/mol) in cyclohexane is 13 nm (above UCEP) which is two times the nanoparticle size $a = 7$ nm. Below UCEP temperature (299 K in this work) the phase diagram for the silica nanoparticle + polystyrene + cyclohexane ternary exhibits a colloid gas (G) phase, colloid gas and liquid (G+L) phases and a colloid liquid (L) phase, depending on the composition. A critical point C1 (G=L) at low polystyrene and silica nanoparticle composition is well established experimentally and theoretically. With the X-ray view cell apparatus phase behavior measurements were reliable up to a polymer mass fraction as high as 0.30. The colloid gas + liquid to colloid liquid (G+L → L) phase boundary arose at smaller silica nanoparticle mass fractions at high polymer mass fraction (> 0.15 mass fraction).

The polystyrene + cyclohexane binary phase diagram shows liquid-liquid phase behavior at 296 K (UCEP = 299 K), from 0.03 to 0.23 mass fraction of polystyrene. As nanoparticles are added, the solvent rich liquid becomes the colloid gas (G) phase. The polystyrene mass fraction in this phase decreases rapidly with nanoparticle mass fraction and underscoring the impact of the depletion flocculation below the UCEP temperature. At 303 K (above UCEP temperature),

polystyrene + cyclohexane binary mixtures are miscible and a single liquid phase is stable. A minimum mass fraction of silica nanoparticles (< 0.005) is needed to induce phase separation. Below this composition limit, polystyrene + cyclohexane mixtures are a colloid gas (G). If the colloid G + L phase region is a closed loop, this requires that two colloid G = colloid L critical points, one at high and one at low polymer mass fraction arise on the two-phase to one-phase boundary. This observed behavior was neither predicted theoretically nor observed experimentally previously. It is a major contribution of this work. The observed diagram, differs both qualitatively and quantitatively from those shown in Chapter 2, Figure 2.8, where at high polymer mass fraction, colloid G is in equilibrium with colloid solid (C), and there is a three-phase colloid G + L + C region.

4.5   Generalization of Phase Diagrams for Nanoparticles + Non-Adsorbing Polymer + Solvent Ternary Mixtures

The phase behaviour of silica nanoparticles + non-adsorbing polystyrene + cyclohexane show significant temperature dependence - particularly in the vicinity of the UCEP of the polystyrene + cyclohexane binary. In this section, the resulting phase diagrams are linked to previously reported phase diagrams by examining potential interactions between colloid L + C phase regions with the observed colloid L + G phase regions.

Case 1: T < UCEP

Below the UCEP, the observed phase diagram includes equilibria between colloid gas (G) and liquid (L) phases, and single-phase L and G regions. Only one critical point, C1, arising from depletion flocculation effects, is observed. Further, the phase diagram shows the interaction between depletion flocculation and molecular liquid-liquid phase separation mechanisms because at intermediate nanoparticle mass fractions, a single colloid liquid phase and not multiple phase regions are observed. A hypothesized phase diagram including high nanoparticle mass fractions, for this case, is shown in Figure 4.10 where the L+C and C regions do not intersect with the L+G region. This diagram links with published diagrams at low radius of gyration of polymer to the particle size ratios (0.1 to 0.3) as shown in Figure 2.7. If the L+C region intersects the L+G region, a phase diagram including these effects is easily envisaged, Figure 4.11, which parallels published phase diagrams for high radius of gyration to particle size ratios (0.4 to 2.2) as shown in Figure 2.5. The diagram shown in Figure 4.11 is likely to arise if the L+G region extends to larger nanoparticle mass fractions. While not observed, this is likely to be a function of temperature and the radius of gyration to particle size ratio.

Figure 4.10. Proposed phase diagram of non-adsorbing polymer + nanoparticles + solvent mixture at T < UCEP.

Figure 4.11. Schematic of a new phase diagram of non-adsorbing polymer + solvent + nanoparticles mixture at T< UCEP.

Case 2: T = UCEP

At the UCEP a second critical point emerges from the polymer mass fraction axis as sketched in Figure 4.12. This second critical point, C2, is incipient and creates an emergent closed loop for the colloid G+L phase region. The first critical point, C1, is temperature and composition invariant and is attributed to depletion flocculation effects. Again, the phase diagram shows the interaction between depletion flocculation and molecular liquid-liquid phase separation mechanisms because at intermediate nanoparticle mass fractions, a single colloid liquid phase and not multiple phase regions are observed. The hypothesized phase diagram including high

nanoparticle mass fractions, for this case, is shown in Figure 4.12 where the L+C and C regions do not intersect with the L+G region. This diagram links with published diagrams at low radius of gyration of polymer to particle size ratio (0.1 to 0.3) as shown in Figure 2.8. If the L+C region intersects the L+G region, a phase diagram including these effects is easily envisaged, Figure 4.13, which parallels published phase diagrams for high ratios of radius of gyration of polymer to particles size as shown in Figure 2.5. The diagram shown in Figure 4.13 is likely to arise if the L+G region extends to larger nanoparticle mass fractions.
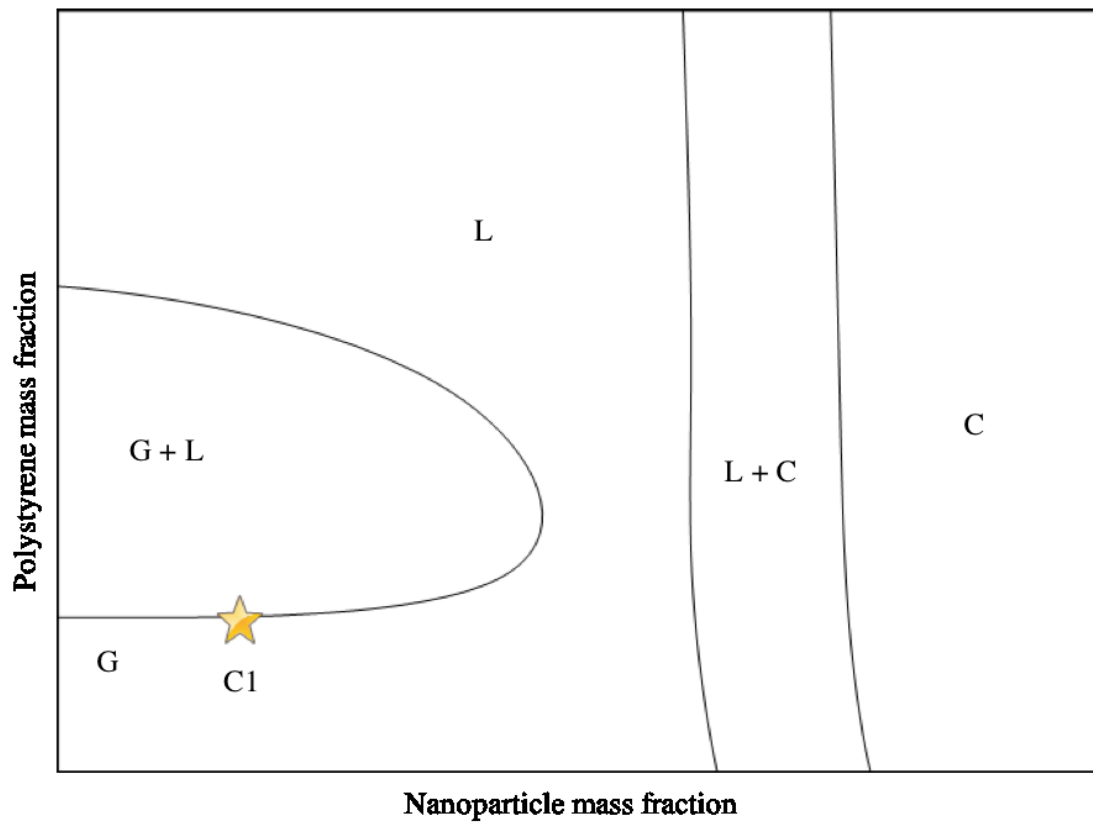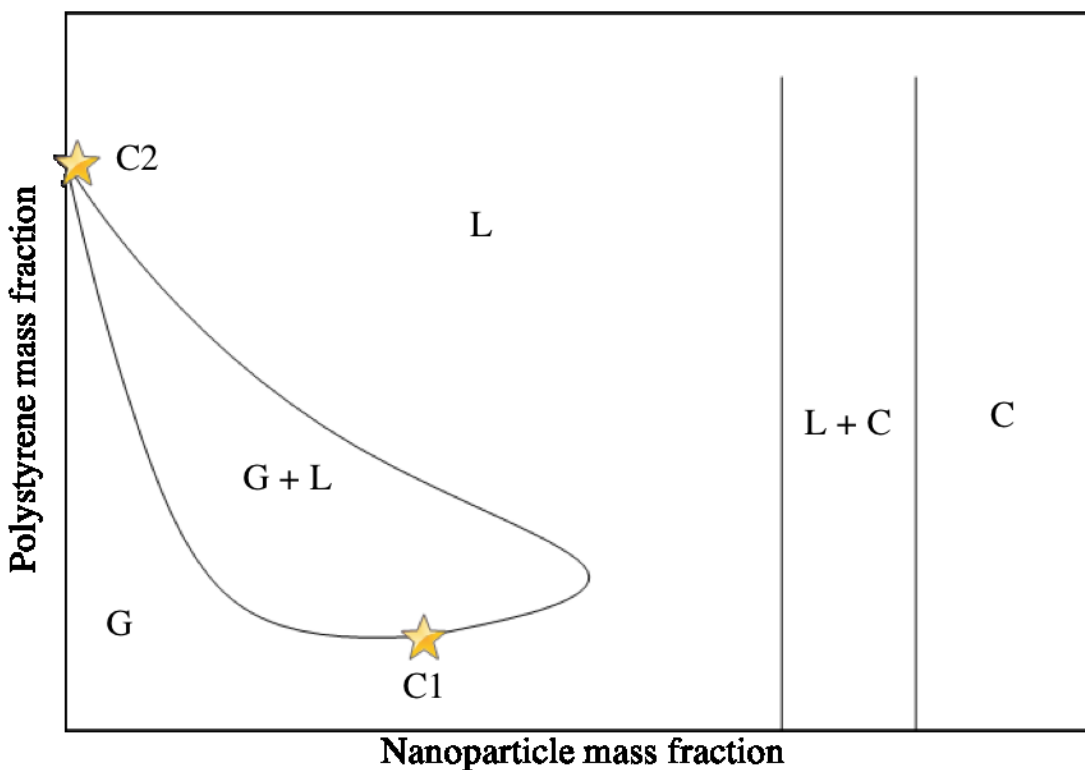

Figure 4.12. Proposed phase diagram of non-adsorbing polymer + nanoparticles + solvent mixture at T = UCEP.
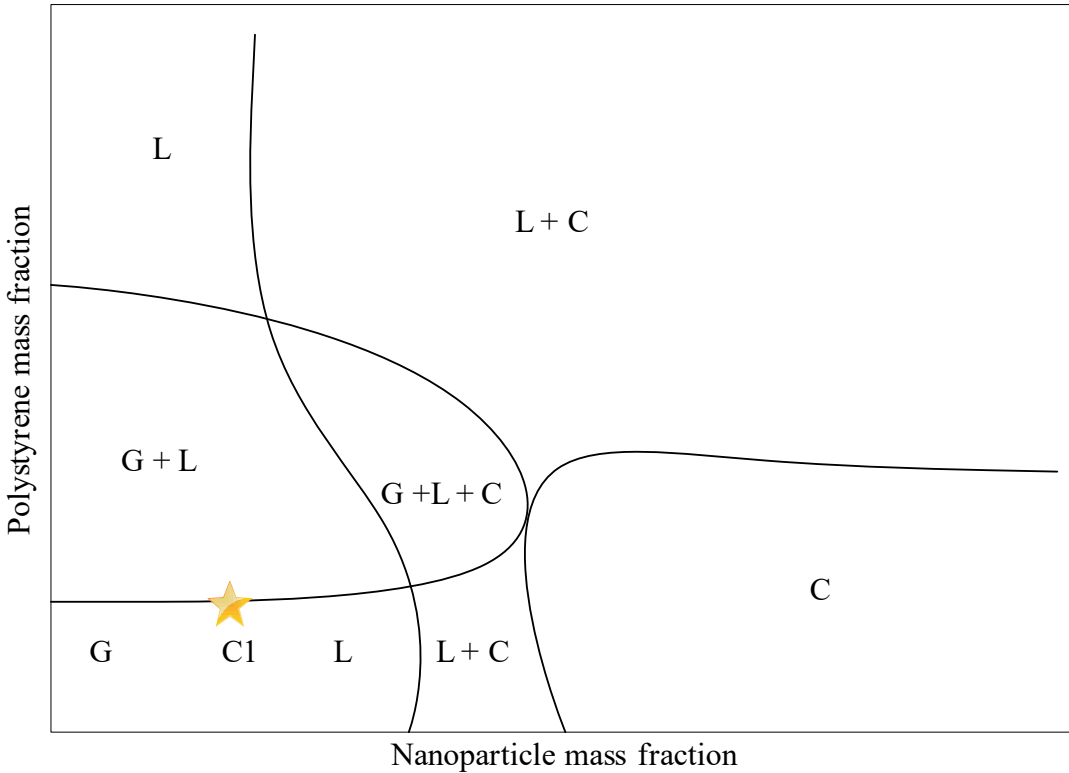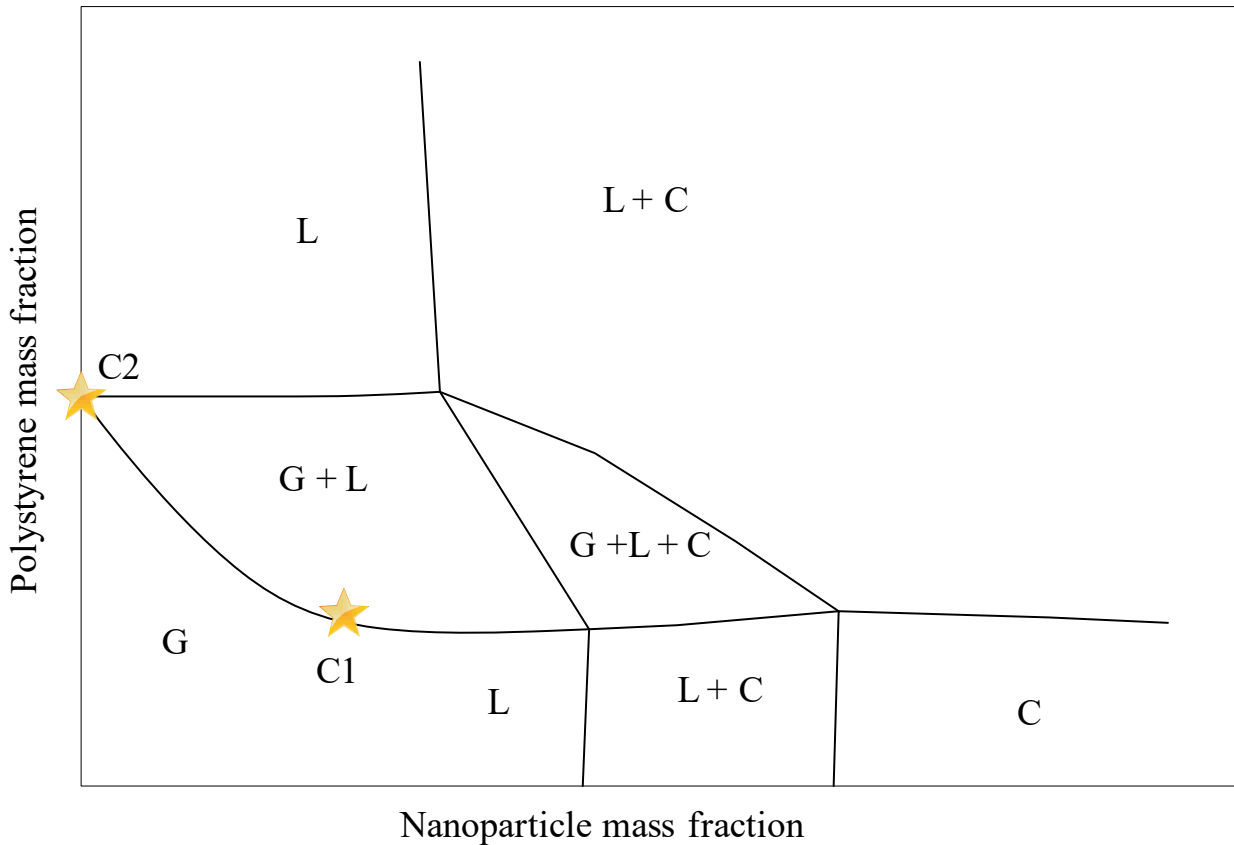
Figure 4.13. Schematic of a new phase diagram for non-adsorbing polymer + solvent + nanoparticles mixture at T=UCEP.

Case 3: T > UCEP

Above the UCEP temperature, the critical point C2 shifts away from the polymer mass fraction axis as shown in Fig. 4.14 (a), creating a colloid gas region at low nanoparticle mass fraction. For the silica nanoparticle + polystyrene + cyclohexane ternary, the C2 critical locus has a trajectory trending toward higher polymer and nanoparticle mass fractions as temperature increases. Critical point C1, from observations and as anticipated from depletion flocculation theory is invariant within measurement uncertainty. The hypothesized phase diagram including

high nanoparticle mass fractions, for this case, Figure 4.14 (a) where the L+C and C regions do not intersect with the L+G region, links with published diagrams at low ratio of radius of gyration of polymer to particle size shown in Figure 2.7. If the L+C and L+G regions intersect, a G+L+C region is created and additional phase diagrams shown in Figures 4.14 (b-d) may arise. Phase diagrams shown in Figures 4.14 (b) and 4.14 (c), are illustrative transitional phase diagrams. In both cases, the critical point C2 is still evident. Only when critical point C2 becomes "buried" by interference from the C, and C+L behaviours is the previously-observed temperature-independent colloidal phase diagram for high ratios (0.4 to 2.2) of radius of gyration of polymer to particle size, Figure 4.14 (d)[9] recovered.
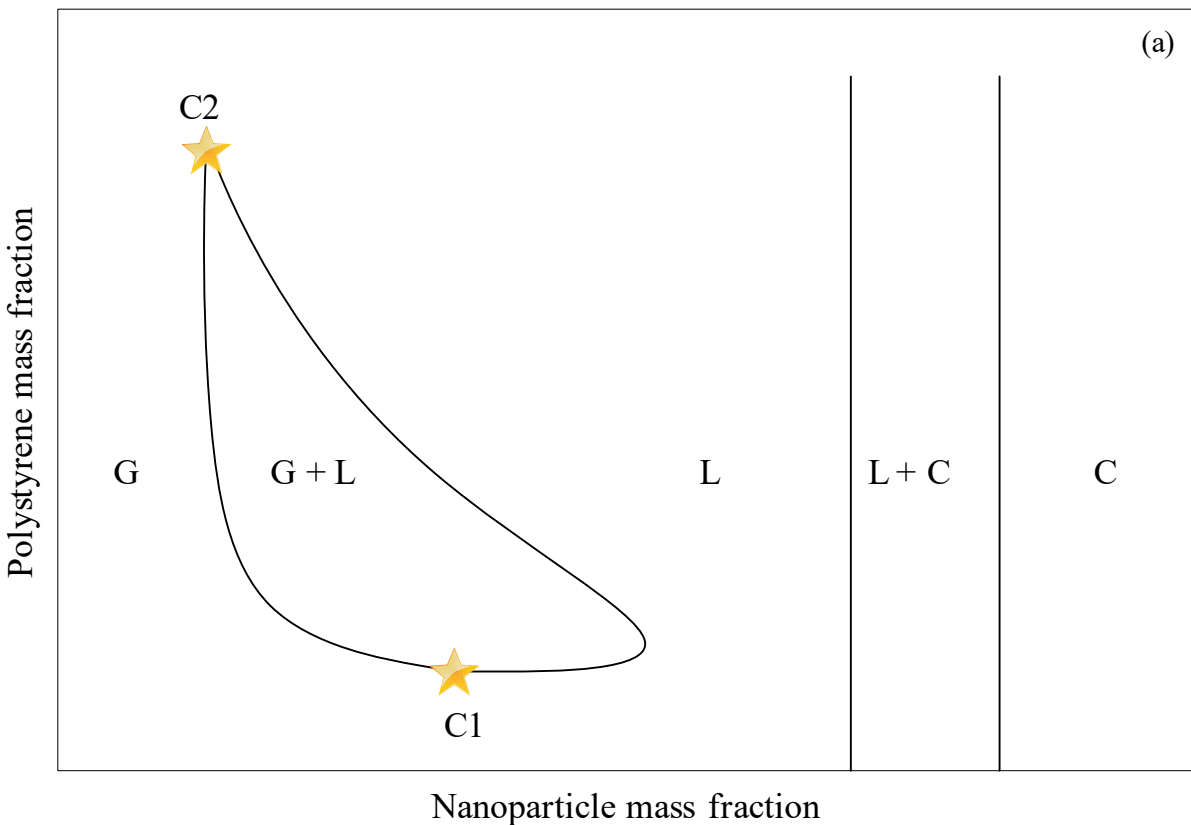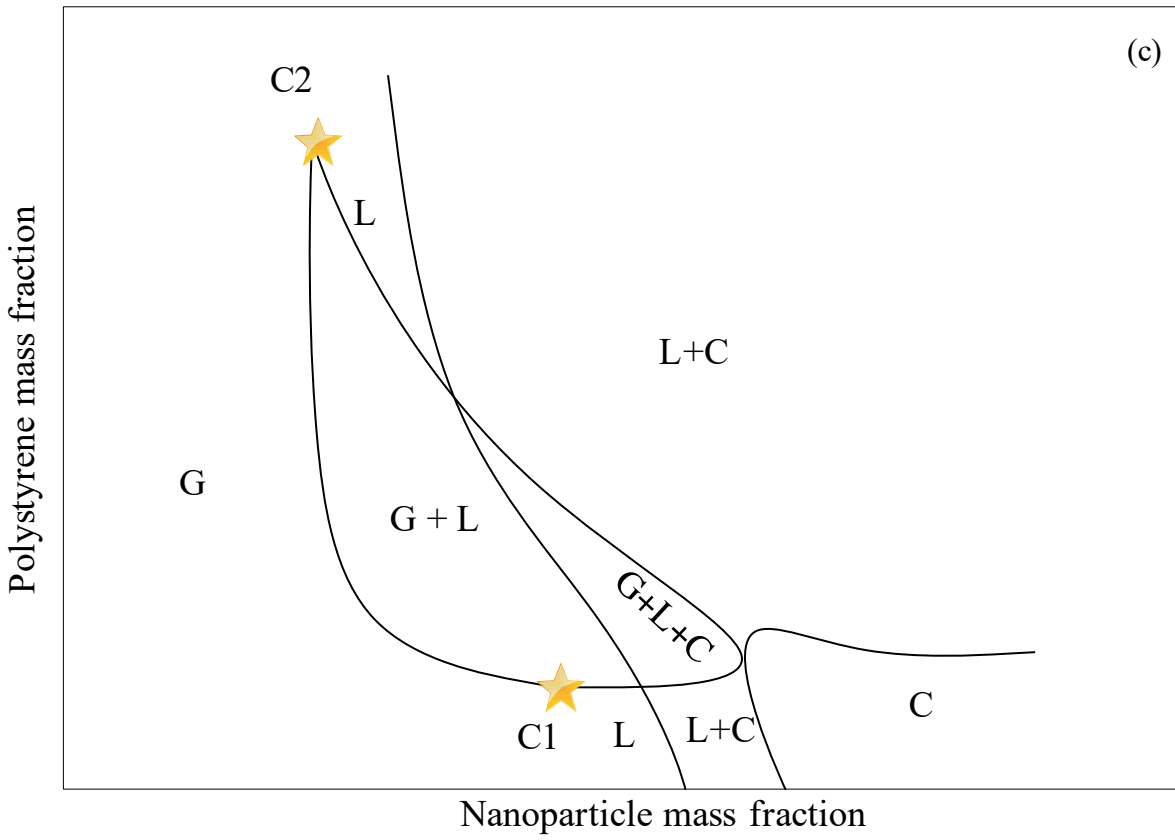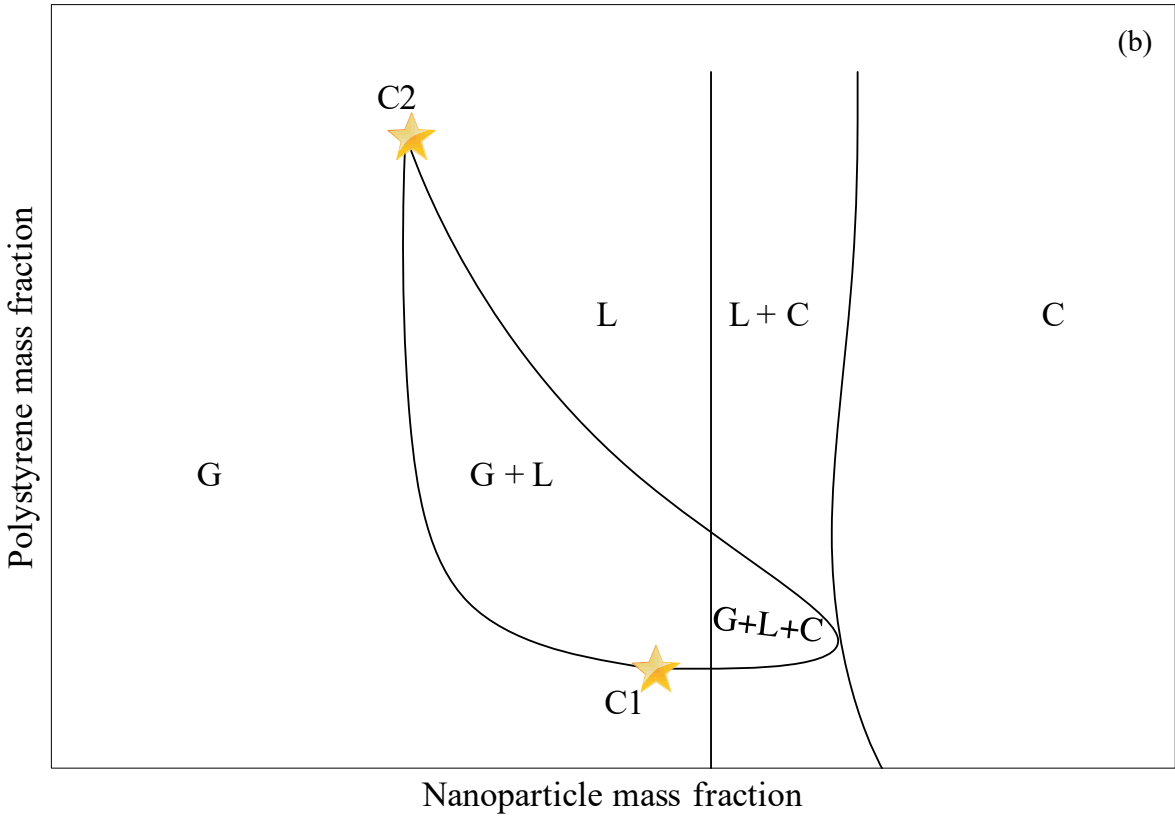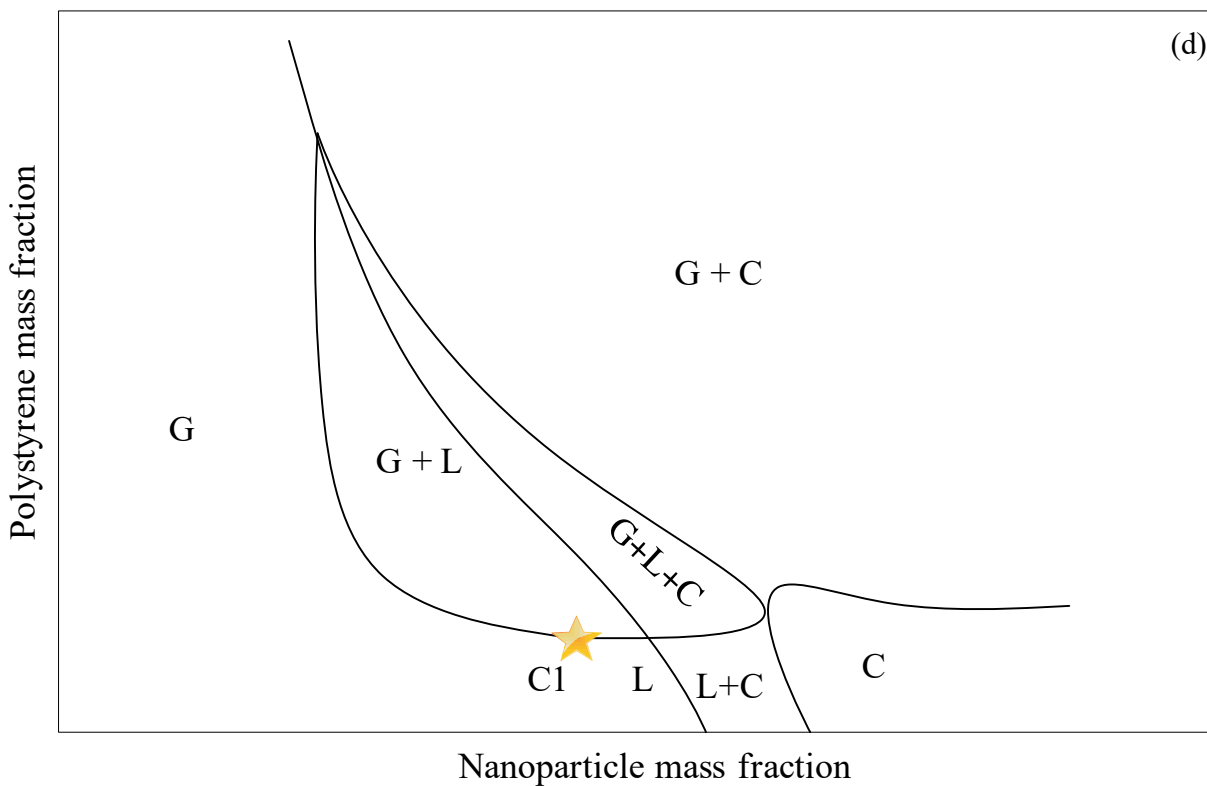
Figure 4.14. Phase diagram schematics for non-adsorbing polymer + solvent + nanoparticle mixtures above the UCEP temperature showing the transition from the phase diagram observed in this work (a), transitional phase diagrams (b) and (c) yet to be observed, and a temperature-invariant colloid phase diagram for high size ratio of radius of gyration of polymer to particles average size published previously (d).[9]

4.6 Nomenclature

MW   molar mass

G   colloid gas like phase

L   colloid liquid like phase

C   particle rich phase

G+C   colloid gas-particle region

G+L   colloid gas-liquid region

L+C   colloid liquid-particle region

G+L+C   colloid gas-liquid-particle region

UCEP   upper critical end point

R_g radius of gyration

a particle size

4.7   References

1.   Terao, K.; Okumoto, M.; Nakamura, Y.; Norisuye, T.; Teramoto, A. Light-scattering and phase-separation studies on cyclohexane solutions of four-arm star polystyrene. Macromolecules **1998**, 31, 6885-6890.

2.   Tsuyumoto, M.; Einaga, Y.; Fujita, H. Phase equilibrium of the ternary system consisting of two monodisperse polystyrenes and cyclohexane. Polym. J. **1984**, 16, 229-240.

3.   Nakata, M.; Kuwahara, N.; Kaneko, M. Coexistence curve for polystyrene–cyclohexane near the critical point. J. Chem. Phys. **1975**, 62, 4278-4283.

4.   Kamide, K.; Matsuda, S.; Dobashi, T.; Kaneko, M. Cloud point curve and critical point of multicomponent polymer/single solvent system. Polym. J. **1984**, 16, 839-855.

5.   Sun, S.; Nishio, I.; Swislow, G.; Tanaka, T. The coil–globule transition: radius of gyration of polystyrene in cyclohexane. J. Chem. Phys. **1980**, 73, 5971-5975.

6.   Vidakovic, P.; Rondelez, F. Temperature dependence of the hydrodynamic radius of flexible coils in solutions. 2. Transition from the θ to the collapsed state. Macromolecules **1984**, 17, 418-425.

7.   Garca, M. T.; Gracia, I.; Duque, G.; de Lucas, A.; Rodrguez, J. F. Study of the solubility and stability of polystyrene wastes in a dissolution recycling process. Waste Manage. **2009**, 29, 1814-1818.

8.   Fleer, G. J.; Tuinier, R. Analytical phase diagrams for colloids and non-adsorbing polymer. Adv. Colloid Interface Sci. **2008**, 143, 1-47.

9.   Anderson, V. J.; Lekkerkerker, H. N. Insights into phase transition kinetics from colloid science. Nature **2002**, 416, 811-815.

Chapter 5. Conclusions and Future Work

5.1   Conclusions

The phase behavior of ternary mixtures of polystyrene, cyclohexane and silica nanoparticles was assessed and is presented in this work. The resulting phase diagrams were discussed in relation to the UCEP temperature of polystyrene + cyclohexane binary mixtures. This subdivision of the data facilitated the discrimination of depletion flocculation and molecular phase separation mechanisms and the establishment of links with the current colloid phase diagram literature. The interplay between molecular and colloidal phase behavior led to phase diagrams that were not previously anticipated for non-adsorbing polymer + solvent + nanoparticle mixtures. Some of these phase diagrams were observed directly. Other phase diagrams are inferred from phase diagram theory as transitional when colloid solid and colloid gas + liquid phase behaviours overlap. For example, above the UCEP temperature, one new phase diagram including two colloid G=L critical points on a closed loop colloid G + L region was observed experimentally. A second phase diagram with a CLG region and two colloid G=L critical points is inferred, but not observed experimentally, based on this work and prior work of others. Below the UCEP temperature, one new phase diagram was observed experimentally and a second new phase diagram was inferred based on measurements in this work and phase diagram theory.

The colloid gas + liquid to colloid liquid or gas phase boundary in the vicinity of the colloid G=L critical point at low polymer mass fraction, and the composition of arising at this critical point are temperature invariant within measurement uncertainty as anticipated from the literature. Other attributes of the phase boundary, including the high mass fraction colloid G=L

critical point are temperature sensitive. For example, at temperatures, just above the UCEP temperature, where polystyrene and cyclohexane are marginally miscible, even the addition of a trace mass fraction of nanoparticles results in a colloid gas + liquid behavior. At higher temperatures, where the polystyrene + cyclohexane binary mixture is miscible, the colloid gas to colloid gas + liquid boundary is expected to shift to larger nanoparticle mass fractions.

5.2   Future Work

Extending the temperature range of the phase behaviour data set for polystyrene + cyclohexane + silica nanoparticles would provide additional detail concerning the behavior of the high polymer mass fraction colloid G=L critical point, C2, and the colloid gas + liquid to colloid gas and colloid liquid phase boundaries more generally. Evaluating phase diagrams for other polymer radius of gyration to the particle size ratios is also a near term future project. Both of these studies can be performed using the existing equipment and protocols.

Observation of the inferred phase diagrams is a priority for longer term future studies. However, it is unclear whether nanoparticle properties, or a combination of nanoparticle, polymer and solvent properties are primary variables. A thorough literature search and exploratory measurements will be starting points for this longer-term aspect of future work.

With the mixture explored in this work, phase boundaries at high nanoparticle mass fractions were not observed. New experimental methodologies and protocols are needed to observe this region of the phase diagram because polystyrene + cyclohexane + nano silica mixtures are viscous at high nanoparticle mass fraction, this led to possible inhomogeneities

during sample preparation, and phase boundaries were not readily identified using the X-ray tomography because of poor signal transmission at high nano silica mass fractions.

Identification of lead industrial examples and implications for them comprise additional priorities. Fields worth exploring are diverse and include formulation in nanomedicine, oil and gas production, transportation and refining, and environmental science. Examples include:

(1)   The possible identification of polymers to separate fine clay particles in oil sands tailings derived from oil sands ores[1] that exploit the findings in this study. This work will be a good starting point for benchmarking and understanding the interactions between water soluble polymers and fine clay particles.

(2)   The possible development of heat transfer fluids that exploit the findings from this work and a parallel rheological investigation. Fluids including nanoparticles have improved thermal conductivity but this effect is often negated by an increase in viscosity. Colloid liquid + colloid gas dispersions/emulsions[2] may not suffer from this latter deficit.

5.3   References

1.   Wang, X. T.; Feng, X.; Xu, Z.; Masliyah, J. H. Polymer aids for settling and filtration of oil sands tailings. Can. J. Chem. Eng. **2010**, 88, 403-410.

2.   Wang, R.; Knudsen, J. G. Thermal conductivity of liquid-liquid emulsions. Ind. Eng. Chem. **1958**, 50, 1667-1670.

Bibliography

❖ Abedi, S. J.; Cai, H. -Y.; Seyfaie, S.; Shaw, J. M. Simultaneous phase behaviour, elemental composition and density measurement using X-ray imaging. Fluid Phase Equilib. **1999**, 158, 775-781.

❖ Amani, M. J.; Gray, M. R.; Shaw, J. M. On correlating water solubility in ill-defined hydrocarbons. Fuel **2014**, 134, 644-658.

❖ Anderson, V. J.; Lekkerkerker, H. N. Insights into phase transition kinetics from colloid science. Nature **2002**, 416, 811-815.

❖ Asakura, S.; Oosawa, F. On interaction between two bodies immersed in a solution of macromolecules. J. Chem. Phys. **1954**, 22, 1255-1256.

❖ Chien, S.; Simchon, S.; Abbott, R. E.; Jan, K. Surface adsorption of dextrans on human red cell membrane. J. Colloid Interface Sci. **1977**, 62, 461-470.

❖ Clarke, J.; Vincent, B. Nonaqueous silica dispersions stabilized by terminally anchored polystyrene: The effect of added polymer. J. Colloid Interface Sci. **1981**, 82, 208-216.

❖ De Boer, D. Fundamental parameters for X-ray fluorescence analysis. Spectrochimica Acta Part B: Atomic Spectroscopy **1989**, 44, 1171-1190.

❖ De Hek, H.; Vrij, A. Phase separation in non-aqueous dispersions containing polymer molecules and colloidal spheres. J. Colloid Interface Sci. **1979**, 70, 592-594.

❖ Dini, Y.; Becerra, M.; Shaw, J. M. Phase Behavior and Thermophysical Properties of Peace River Bitumen Propane Mixtures from 303 K to 393 K. J. Chem. Eng. Data **2016**, 61, 2659-2668.

❖ Emmett, S.; Vincent, B. Phase separation in dispersions of weakly interacting particles induced by non-adsorbing polymer. Phase Transitions: A Multinational Journal **1990**, 21, 197-206.

❖ Fetters, L. J.; Hadjichristidis, N.; Lindner, J. S.; Mays, J. W. Molecular Weight Dependence of Hydrodynamic and Thermodynamic Properties for Well-Defined Linear Polymers in Solution. J. Phys. Chem. Ref. Data **1994**, 23, 619-640.

❖ Fleer, G. J.; Tuinier, R. Analytical phase diagrams for colloids and non-adsorbing polymer. Adv. Colloid Interface Sci. **2008**, 143, 1-47.

❖ Flory, P.; Cherayil, B. Spatial configuration of macromolecular chains. Reson **2003**, 8, 82-90.

❖ Garca, M. T.; Gracia, I.; Duque, G.; de Lucas, A.; Rodrguez, J. F. Study of the solubility and stability of polystyrene wastes in a dissolution recycling process. Waste Manage. **2009**, 29, 1814-1818.

❖ Gençaslan, M.; Bilgin, Y.; Keskin, M. Systematic investigation of the global phase behavior of polymer–solvent systems in the density–density plane. Fluid Phase Equilib. **2011**, 301, 191-199.

❖ Geschke, D. Physical Properties of Polymers Handbook. Zeitschrift fr Physikalische Chemie **1997**, 199, 128.

❖ Hiemenz, P. C.; Rajagopalan, R. Principles of Colloid and Surface Chemistry, revised and expanded; CRC press: **1997**; Vol. 14.

❖ Ilett, S. M.; Orrock, A.; Poon, W.; Pusey, P. N. Phase behavior of a model colloid-polymer mixture. Physical Review E **1995**, 51, 1344.

❖ Jenkins, P.; Snowden, M. Depletion flocculation in colloidal dispersions. Adv. Colloid Interface Sci. **1996**, 68, 57-96.

❖ Kamide, K.; Matsuda, S.; Dobashi, T.; Kaneko, M. Cloud point curve and critical point of multicomponent polymer/single solvent system. Polym. J. **1984**, 16, 839-855.

❖ Khammar, M.; Shaw, J. M. Estimation of Phase Composition and Size of Asphaltene Colloidal Particles in Mixtures of Asphaltene + Polystyrene + Toluene at 293 K and Atmospheric Pressure. Fluid Phase Equilib. **2012**, 332, 105-119.

❖ Khammar, M.; Shaw, J. M. Liquid-Liquid Phase Equilibria in Asphaltene + Polystyrene + Toluene Mixtures at 293 K, Energy & Fuels **2012**, 26(2), 1075-1088.

❖ Kok, C. M.; Rudin, A. Relationship between the hydrodynamic radius and the radius of gyration of a polymer in solution. Macromolecular Rapid Communications **1981**, 2, 655-659.

❖ Koningsveld, R.; Kleintjens, L. A. Liquid-liquid phase separation in multicomponent polymer systems. X. Concentration dependence of the pair-interaction parameter in the system cyclohexane-polystyrene. Macromolecules **1971**, 4, 637-641.

❖ Koningsveld, R.; Kleintjens, L. A.; Shultz, A. R. Liquid–liquid phase separation in multicomponent polymer solutions. IX. Concentration-dependent pair interaction parameter from critical miscibility data on the system polystyrene–cyclohexane. Journal of Polymer Science Part A-2: Polymer Physics **1970**, 8, 1261-1278.

❖ Konynenburg, P. H. V.; Scott, R. L. Critical Lines and Phase Equilibria in Binary Van Der Waals Mixtures. Philos. Trans. R. Soc. Lond. A **1980**, 298, 495.

❖ Kuwahara, N.; Nakata, M.; Kaneko, M. Cloud-point curves of the polystyrene-cyclohexane system near the critical point. Polymer **1973**, 14, 415-419.

❖ Lekkerkerker, H.; Poon, W.; Pusey, P. N.; Stroobants, A.; Warren, P. 0. Phase behaviour of colloid polymer mixtures. EPL (Europhysics Letters) **1992**, 20, 559.

❖ Lynch, I.; Cornen, S.; Piculell, L. Investigation of the segregative phase separation induced by addition of polystyrene to AOT oil-continuous microemulsions. J. Phys. Chem. B **2004**, 108, 5443-5452.

❖ Matsuda, H.; Fujita, M.; Ochi, K. Measurement and correlation of mutual solubilities for high-viscosity binary systems: aniline methylcyclohexane, phenol heptane, phenol octane, and glycerol 1-pentanol. J. Chem. Eng. Data **2003**, 48, 1076-1080.

❖ McHugh, M.; Krukonis, V. Supercritical fluid extraction: principles and practice; Elsevier: **2013**.

❖ Nakata, M.; Kuwahara, N.; Kaneko, M. Coexistence curve for polystyrene–cyclohexane near the critical point. J. Chem. Phys. **1975**, 62, 4278-4283.

❖ Ogden, A. L.; Lewis, J. A. Effect of nonadsorbed polymer on the stability of weakly flocculated suspensions. Langmuir **1996**, 12, 3413-3424.

❖ Pizer, S. M.; Amburn, E. P.; Austin, J. D.; Cromartie, R.; Geselowitz, A.; Greer, T.; ter Haar Romeny, B.; Zimmerman, J. B.; Zuiderveld, K. Adaptive histogram equalization and its variations. Computer vision, graphics, and image processing **1987**, 39, 355-368.

❖ Poon, W. The physics of a model colloid–polymer mixture. J. Phys.: Condens. Matter **2002**, 14, R859.

❖ Pouralhosseini, S.; Shaw, J. M. Temperature-Independent Colloidal Phase Behavior of Maya Asphaltene + Toluene + Polystyrene Mixtures. Energy & Fuels **2015**, 29(8), 4864-4873.

❖ Ramakrishnan, S.; Fuchs, M.; Schweizer, K. S.; Zukoski, C. F. Entropy driven phase transitions in colloid–polymer suspensions: Tests of depletion theories. J. Chem. Phys. **2002**, 116, 2201-2212.

❖ Saeki, S.; Kuwahara, N.; Konno, S.; Kaneko', M. Upper and Lower Critical Solution Temperatures in Polystyrene Solutions. Macromolecules **1973**, 6, 246-250.

❖ Sanchez, I. C.; Lacombe, R. H. Statistical thermodynamics of polymer solutions. Macromolecules **1978**, 11, 1145-1156.

❖ Shultz, A. R.; Flory, P. J. Phase Equilibria in Polymer—Solvent Systems1, 2. J. Am. Chem. Soc. **1952**, 74, 4760-4767.

❖ Sperry, P. R. Morphology and mechanism in latex flocculated by volume restriction. J. Colloid Interface Sci. **1984**, 99, 97-108.

❖ Stahl, G. A.; Schulz, D. N. Water-soluble polymers for petroleum recovery; Springer Science & Business Media: **2012**; .

❖ Sun, S.; Nishio, I.; Swislow, G.; Tanaka, T. The coil–globule transition: radius of gyration of polystyrene in cyclohexane. J. Chem. Phys. **1980**, 73, 5971-5975.

❖ Tadros, T. F.; Zsednai, A. Application of depletion flocculation for prevention of formation of dilatant sediments. Colloids and Surfaces **1990**, 43, 105-116.

❖ Terao, K.; Okumoto, M.; Nakamura, Y.; Norisuye, T.; Teramoto, A. Light-scattering and phase-separation studies on cyclohexane solutions of four-arm star polystyrene. Macromolecules **1998**, 31, 6885-6890.

❖ Tsuyumoto, M.; Einaga, Y.; Fujita, H. Phase equilibrium of the ternary system consisting of two monodisperse polystyrenes and cyclohexane. Polym. J. **1984**, 16, 229-240.

❖ Vidakovic, P.; Rondelez, F. Temperature dependence of the hydrodynamic radius of flexible coils in solutions. 2. Transition from the θ to the collapsed state. Macromolecules **1984**, 17, 418-425.

❖ Vincent, B.; Edwards, J.; Emmett, S.; Croot, R. Phase separation in dispersions of weakly-interacting particles in solutions of non-adsorbing polymer. Colloids and Surfaces **1988**, 31, 267-298.

❖ Vincent, B.; Edwards, J.; Emmett, S.; Jones, A. Depletion flocculation in dispersions of sterically-stabilised particles ("soft spheres"). Colloids and Surfaces **1986**, 18, 261-281.

❖ Vrij, A. Polymers at interfaces and the interactions in colloidal dispersions. Pure and Applied Chemistry **1976**, 48, 471-483.

❖ Wünsch, Josef Richard. Polystyrene: Synthesis, production and applications. Vol. 112. iSmithers Rapra Publishing, **2000**.

❖ Zou, X. Selective removal of inorganic fine solids, heavy metals and sulfur from bitumen/heavy oils; University of Toronto: **2003**.

❖ Zou, X.; Zhang, X.; Shaw, J. Phase Behavior of Athabasca Vacuum Bottoms + n-Alkane Mixtures. SPE Production & Operations **2007**, 22, 265-272.

❖ Wang, X. T.; Feng, X.; Xu, Z.; Masliyah, J. H. Polymer aids for settling and filtration of oil sands tailings. Can. J. Chem. Eng. **2010**, 88, 403-410.

❖ Wang, R.; Knudsen, J. G. Thermal conductivity of liquid-liquid emulsions. Ind. Eng. Chem. **1958**, 50, 1667-1670.

Supplementary Materials

❖ Video showing the transition from one phase to two phases of the (1:9) polystyrene:

cyclohexane control mixture

(URL:https://drive.google.com/file/d/1RGqkSRF-

4rtO__TBLVIKBC5Dg6EGBbTw/view?usp=sharing)